M A T H E M A T I C S D E P A R T M E N T

On Spurious Asymptotic Numerical Solutions of 2×2 Systems of ODEs[1]

P.K. Sweby
&
H.C. Yee[2]

Numerical Analysis Report 7/91

October 1991

U N I V E R S I T Y O F R E A D I N G

[1]The majority of this work was performed whilst the first author was a visiting scientist at the NASA Ames Research Center.

[2]Staff Scientist, Fluid Dynamics Division, NASA Ames Research Center, Moffett Field, CA 94035,USA

Abstract

The phenomenon that the asymptotic behaviour of a nonlinear differential equation and its discretized counterpart can have different dynamical behavior was not uncovered fully until recently. In our earlier work we discussed some of the differences between the dynamics of scalar first-order autonomous nonlinear ODEs and commonly used ODE solvers. In this report we investigate (largely) numerically the dynamical behavior of numerical discretizations of 2 x 2 systems of first-order autonomous nonlinear ODEs. Our goal is to illustrate the interplay between the occurrence of spurious fixed points, limit cycles and numerical basins of attraction, and the phenomenon of incorrect, non-convergent and divergent numerical solutions of a class of Runge-Kutta methods.

1 Introduction

Until recently it was not fully appreciated that the dynamical behaviour of a numerical discretisation of a non-linear differential equation is not necessarily the same as the dynamics of the original equation itself. Iserles [11] showed that whilst linear multistep methods for solving ODEs possess only the fixed points of the original differential equations, popular Runge-Kutta methods may exhibit additional, spurious, fixed points. It has been demonstrated (see for example [17, 7, 19] for the scalar case, and [12, 13] for nonlinear reaction-convection model equations) that such spurious fixed points may be stable below the linearised stability limit of the scheme and, although Humphries [10] has recently shown that if such stable spurious fixed points exist as the time-step approaches zero they must either approach a true fixed point or become unbounded, these spurious features may greatly affect the dynamical behaviour of the numerical solution in practice due to the use of a finite timestep. Indeed this will be the case not only for stable spurious fixed points but also for unstable spurious fixed points and spurious higher order features such as period 2 solutions or even chaos which can be admitted by even the Linear Multistep methods, including the simple Euler scheme. (Hairer *et al* [9] have studied classes of "regular" methods which do not exhibit spurious period one or period two fixed points.)

In [17, 7, 19] we demonstrated the occurrence of spurious fixed points for scalar ODEs when discretised by various numerical schemes. In this report and [18] we investigate, largely numerically, the dynamics of numerical discretisations of 2×2 systems of first-order autonomous nonlinear ODEs, illustrating how wrong, non-convergent or no solutions may be obtained for the discretised equation due to spurious fixed points, limit cycles and numerical basins of attraction respectively. As in the scalar case these phenomena may occur below or very closed to the linearised stability limits of the schemes (itself not always easily calculated). Our ultimate goal is to study and fully appreciate the dynamics of discretisations of PDEs and how it relates to the dynamics of the PDEs themselves, in particular where time-stepping techniques are used to reach a steady-state; preliminary work on this has already commenced ([6, 12, 13]). It is important to remember that not only the discretisations but also preconditioners and relaxation techniques may also modify the dynamics of the original PDE.

In Section 2 we briefly review some basic bifurcation theory before introducing our test cases in Section 3. In Section 4 we proceed to investigate the dynamics of various Runge-Kutta methods applied to our model equations, summarizing our findings in Section 5. Finally, in the Appendix, we describe the techniques used to obtain our detailed pictures of solution orbits and basins of attraction on a Connection Machine CM2.

2 Preliminaries

Before embarking on a description of the systems which we will use as illustrations and the numerical methods which we shall apply to them we review some of the basic theory of fixed points and their bifurcations (see for example [8, 4] for a detailed account).

Consider a systems of ODEs

$$\dot{\mathbf{u}} = \mathbf{F}(\mathbf{u}). \tag{1}$$

This system will have fixed points given by

$$\mathbf{F}(\mathbf{u}_E) = 0 \tag{2}$$

where the subscript "E" stands for "Essential" denoting a fixed point of the ODE as opposed to the additional fixed points of the discretisations which we will encounter later.

A fixed point may be either stable or unstable, i.e. $\mathbf{u}$ given by (1) will either remain in the neighbourhood of the fixed point or move away from it under small perturbations. If we consider such a small perturbation $\boldsymbol{\epsilon}$ with $\mathbf{u} = \mathbf{u}_E + \boldsymbol{\epsilon}$ then a Taylor expansion of (1) yields

$$\dot{\boldsymbol{\epsilon}} = J(\mathbf{u}_E)\boldsymbol{\epsilon} + O(\epsilon^2) \tag{3}$$

where J is the Jacobian matrix

$$J(\mathbf{u}) = \frac{\partial \mathbf{F}}{\partial \mathbf{u}}. \tag{4}$$

This equation (assuming $J(\mathbf{u}_E) \neq 0$ and neglecting the higher order terms) has solution

$$\boldsymbol{\epsilon} = e^{J(\mathbf{u}_E)t}\boldsymbol{\epsilon}_0 \tag{5}$$

with the exponential matrix having eigenvalues $e^{\lambda t}$, λ being the eigenvalues of J. Therefore for the perturbation to decrease, i.e. for the fixed point to be stable, the eigenvalues of J must have negative real parts.

Unlike for the scalar case [17, 7] fixed points for 2×2 (and higher order) systems can be of different type, each type exhibiting a distinctive behaviour (see e.g. [1, 2, 3]). The particular type of fixed point is determined by the eigenvalues of the Jacobian J evaluated at the fixed point. For 2×2 first-order ODEs, if the eigenvalues are real and both of the same sign then the fixed point is called a node, whilst if they are of opposite sign then the fixed point is a saddle. For a saddle one eigenvalue will be positive, the other negative, and so although unstable overall there will be a pair of separatrices, given by the eigenvector of the negative eigenvalue, along which the fixed point is an attractor, see Figure 1. If, however, the eigenvalues are complex then the

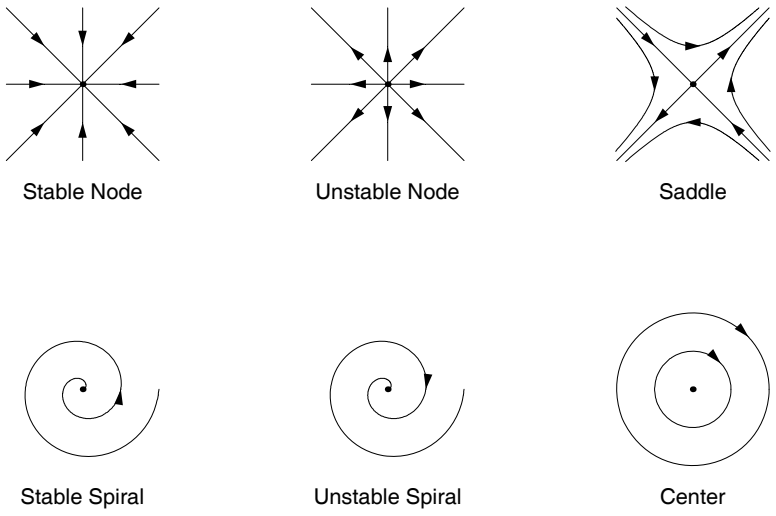

Figure 1: Types of fixed points for a linear 2×2 system.

fixed point is a spiral due to the rotational (sin and cos) terms thus introduced in (5), the "tightness" of the spiral being governed by the magnitude of the imaginary part of the eigenvalues. Finally, if the eigenvalues both have a zero real part the fixed point is non-hyperbolic in nature with neutral stability. Such a fixed point is called a center. The various stable and unstable types are depicted in Figure 1, together with phase trajectories to illustrate the behaviour of values near the fixed points. Note, however, that the behaviour illustrated is only local, the linearisation not being valid globally. For higher order systems a spiral can not exist in isolation but will be combined with another type, e.g. a saddle spiral.

Given a stable fixed point we call the set of all initial values for which the solution trajectory of (1) converges to the same fixed point the "Basin of Attraction" for that particular fixed point. Such a basin may be totally connected or consist of a number of disjoint pieces. Sometimes the boundary of these basins may also appear fractal in nature (see e.g. Figures 13 & 33).

If, due to a variation of a parameter of the ODE, a fixed point becomes unstable then if at the point of instability the eigenvalues are simple and real then the resulting bifurcation will be to another fixed point. If however the eigenvalues are complex then the bifurcation will be of Hopf type. This is a slightly simplified classification since we are not really concerned with variation of the ODE parameters in this work, however full details can be found, for example, in [8] and [4].

We are concerned with the numerical approximation of (1) by an ODE solver. For simplicity we shall restrict ourselves to two level schemes, in particular to Runge-Kutta schemes. For our general analysis we shall write

such a scheme in the form

$$\mathbf{u}^{n+1} = \mathbf{u}^n + r\mathbf{G}(\mathbf{u}^n) \tag{6}$$

where superscripts denote the time level (e.g. $n\Delta t$) and we use r to represent the time-step Δt but allowing it to include any constant scaling factors present in $\mathbf{F}$. The vector function $\mathbf{G}$ is assumed consistent with the ODE in the sense that $\mathbf{F}(\mathbf{u}_E) = 0 \Rightarrow \mathbf{G}(\mathbf{u}_E) = 0$, i.e. that fixed points of the ODE are fixed points of the scheme. Note that in general the converse does not hold, the scheme possessing fixed points which are not fixed points of the ODE (see e.g. [11, 19, 17, 7]). It is this feature which forms the core of our work.

The scheme (6) has fixed points $\mathbf{G}(\mathbf{u}_N) = 0$ which may be true fixed points of (1) $\mathbf{u}_E$ or spurious fixed points $\mathbf{u}_S$. If we perform a perturbation analysis on (6) about $\mathbf{u}_N$ then we obtain

$$\boldsymbol{\epsilon}^{n+1} = \boldsymbol{\epsilon}^n + r\frac{\partial \mathbf{G}(\mathbf{u}_N)}{\partial \mathbf{u}}\boldsymbol{\epsilon}^n + O(\epsilon^2) \tag{7}$$

which, ignoring higher order terms, has solution

$$\boldsymbol{\epsilon}^{n+1} = (I + r\frac{\partial \mathbf{G}(\mathbf{u}_N)}{\partial \mathbf{u}})^{n+1}\boldsymbol{\epsilon}^0. \tag{8}$$

Therefore, for the numerical fixed point $\mathbf{u}_N$ to be stable the eigenvalues of the matrix (assuming $\partial\mathbf{G}(\mathbf{u}_N)/\partial\mathbf{u} \neq 0$)

$$(I + r\frac{\partial \mathbf{G}(\mathbf{u}_N)}{\partial \mathbf{u}}) \tag{9}$$

must lie inside the unit circle. As for the ODE, the relative positioning of the eigenvalues (considering a 2×2 system) determines the type of fixed point. If both eigenvalues are real and both lie inside/outside the unit circle then the fixed point is a stable/unstable node. If one is inside the unit circle, the other outside, then the fixed point is a saddle and if they are complex then the fixed point is a spiral. The situation of eigenvalues on the unit circle (not varying with parameters of the system) is in general indeterminent.

When a fixed point of the discrete map becomes unstable, usually through variation of r, then one of three situations can occur. If the eigenvalue passing outside the unit circle is -1 then a "flip" or "period doubling" bifurcation occurs, however if the eigenvalue is $+1$ then the bifurcation is to another steady state. This bifurcation can either be transcritical (the branches extending both above and below the bifurcation in parameter space) or pitchfork (either subcritical or supercritical), the exact nature depending on higher order terms, see e.g. [7] or [17] for a scalar exposition. If the eigenvalues are complex then (with a few exceptions - see [8]) a Hopf bifurcation occurs. Again

the reader is encouraged to refer to [8] and [4] for full details. The stability of bifurcation branches is established in a similar fashion as above, with usually only portions of the branches being stable.

Finally another feature which can arise (for both a system of ODEs and their discretisation), usually as the result of a Hopf bifurcation, is a limit cycle where the map traverses a closed curve in phase space. In all but a few simple cases such limit cycles are beyond analysis.

3 The equations

In this present work we restrict ourselves to four non-linear systems of ODEs to illustrate the modified dynamics of our ODE solvers over the dynamics of the original differential equations. Two of these systems arise from the mathematical modelling of physical and biological processes, namely a damped pendulum and a simple model of predator-prey interaction in population dynamics. A third system arises as a gross simplification of a PDE solver (our ultimate objective). We emphasise, however, that since the purpose is to illustrate the type of spurious dynamics that may be introduced by ODE solvers we do not always restrict our examples to their regions of physical relevance. Neither do we treat any parameter present in the differential equations as a bifurcation parameter but keep it constant throughout each numerical calculation and so only the discretisation parameters come into play.

The systems considered are

1. A **Predator-Prey** model:

$$\begin{aligned} \dot{u} &= -3u + 4u^2 - \tfrac{1}{2}uv - u^3 \\ \dot{v} &= -2.1v + uv \end{aligned} \tag{10}$$

2. A **Damped Pendulum** model:

$$\begin{aligned} \dot{u} &= v \\ \dot{u} &= -\beta v - \sin(u) \end{aligned} \tag{11}$$

3. A **Dissipative Complex** equation:

$$\dot{z} = z(i + \beta - |z|^2) \tag{12}$$

   where $z = u + iv$

4. A **Perturbed Hamiltonian** system:

$$\begin{aligned} \dot{u} &= \beta(1 - 3u) - \tfrac{3}{4}(1 - 2u + u^2 - 2v(1 - u)) \\ \dot{v} &= \beta(1 - 3v) + \tfrac{3}{4}(1 - 2v + v^2 - 2u(1 - v)) \end{aligned} \tag{13}$$

fixed point	eigenvalues	type	eigenvectors
$(0,0)$	$-3,\ -2.1$	Stable Node	
$(1,0)$	$-1.1,\ 2$	Saddle	$(1,6.2)^T,\ (1,0)^T$
$(3,0)$	$-6,\ 0.9$	Saddle	$(1,0)^T,\ (1,-4.6)^T$
$(2.1,1.98)$	$-0.21 \pm i\sqrt{2.0349}$	Stable Spiral	

Table 1: The fixed points of the Predator-Prey equations.

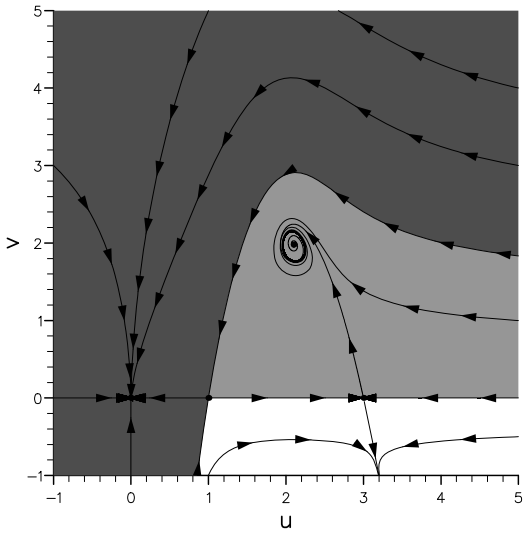

Figure 2: Phase plane for the Predator-Prey equations.

We now study the dynamical behaviour of each system so that we can later distinguish the additional dynamics introduced by our discretisations.

The Predator-Prey system (10) has fixed points ($\dot{u} = \dot{v} = 0$) $(0,0)$, $(1,0)$, $(3,0)$ and $(2.1, 1.98)$ and a Jacobian

$$J = \begin{pmatrix} -3 + 8u - \frac{1}{2}v - 3u^2 & -\frac{1}{2}u \\ v & u - 2.1 \end{pmatrix}. \tag{14}$$

Direct substitution of the fixed points into the Jacobian yields its eigenvalues and thus classifies the fixed points as in Table 1. The eigenvectors, where given, indicate the stable and unstable saddle trajectories (locally) and the global picture is given in the phase portrait of Figure 2. The shaded regions indicate the basins of attraction of the node and spiral. Initial data within these regions will converge asymptotically towards the respective attractor, whilst initial data in the unshaded region will not converge to a fixed point.

Due to the periodicity of the sin term, the Damped Pendulum equation (11) has an infinite number of fixed points, namely $(k\pi, 0)$ for integer k. The

fixed point	eigenvalues	type	eigenvectors
$((2m+1)\pi, 0)$	$\frac{-\beta \pm \sqrt{\beta^2+4}}{2}$	Saddles	$(1, \lambda_1)^T$, $(1, \lambda_2)^T$
$(2m\pi, 0)$	$\frac{-\beta \pm \sqrt{\beta^2-4}}{2}$	Stable Spirals $\beta < 2$ Stable Nodes $\beta \geq 2$	

Table 2: The fixed points of the Damped Pendulum equation.

Jacobian of this system is

$$J = \begin{pmatrix} 0 & 1 \\ -\cos(u) & -\beta \end{pmatrix} \tag{15}$$

which, at the fixed points, has eigenvalues

$$\lambda = \frac{-\beta \pm \sqrt{\beta^2 - 4(-1)^k}}{2}. \tag{16}$$

If k is odd then it is easily seen that the eigenvalues are of opposite sign and so these fixed points are saddles. If k is even, however, two cases must be considered depending on the value of β. If $\beta < 2$ the eigenvalues are complex, with negative real part, and so the fixed points are attracting spirals, if on the other hand $\beta \geq 2$ the eigenvalues are real and negative and so the fixed point is a node. The situation is summarised in Table 2 and Figure 3.

The Dissipative Complex equation (12) is included in our examples since as well as a fixed point it possesses an analytical limit cycle. The fixed point is at $(0, 0)$ and since the Jacobian of the equation, treated as a real system by writing $z = u + iv$, is given by

$$J = \begin{pmatrix} \beta - 3u^2 - v^2 & -1 - 2uv \\ 1 - 2uv & \beta - 3v^2 - u^2 \end{pmatrix} \tag{17}$$

it is easily seen that this fixed point is a stable spiral for $\beta < 0$ and an unstable spiral for $\beta > 0$. The limit cycle can (unusually) be found analytically for this system. Considering the equation in its original (complex) form we have

$$\begin{aligned} \bar{z}\dot{z} + z\dot{\bar{z}} = \frac{d|z|^2}{dt} &= 2|z|^2(\beta - |z|^2) \\ &= 0 \text{ if } |z|^2 = \beta \end{aligned} \tag{18}$$

and so the orbit $|z| = \sqrt{\beta}$ is a limit cycle, that is, it is a closed solution trajectory of the system. A perturbation analysis readily shows that this limit cycle is stable (in an intuitive sense) for all (positive) β. Table 3 and Figure 4 summarise the behaviour of this system.

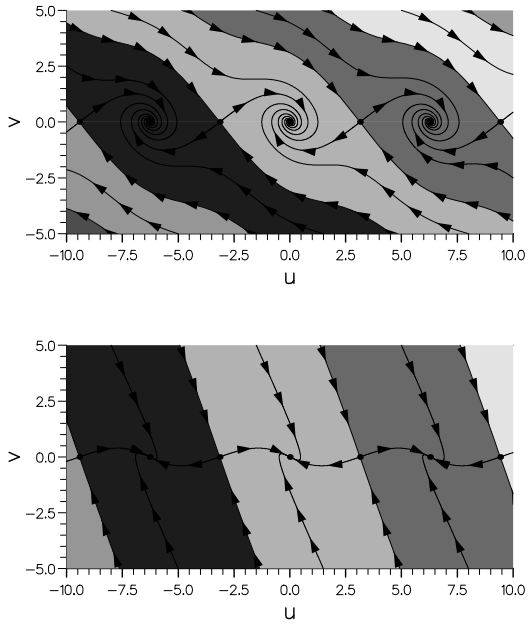

Figure 3: Phase plane for the Damped Pendulum, $\beta < 2$ (top) and $\beta > 2$ (bottom).

orbit	eigenvalues	type
$(0,0)$	$\beta \pm i$	Stable Spiral $\beta < 0$
		Center $\beta = 0$
		Unstable Spiral $\beta > 0$
$\|z\| = \sqrt{\beta}$		Stable Limit Cycle ($\beta > 0$)

Table 3: The dynamics of the Dissipative Complex equation.

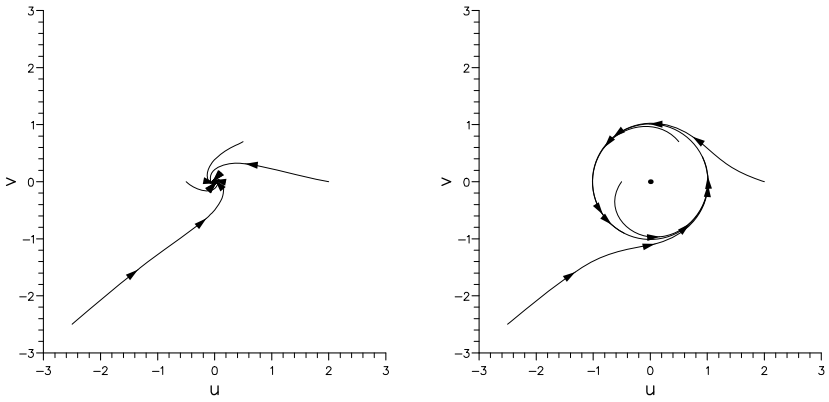

Figure 4: Phase plane for the Dissipative Complex equation, $\beta < 0$ (left) and $\beta > 0$ (right).

Before investigating the behaviour of the Perturbed Hamiltonian system (13) we show its relationship with the numerical solution of a PDE. Consider the viscous Burger's equation

$$u_t + (\tfrac{1}{2}u^2)_x = \epsilon u_{xx} \tag{19}$$

in a semi-discrete framework with spatial derivatives approximated by centered differences, i.e.

$$\dot{u}_k + \frac{\frac{1}{2}u_{k+1}^2 - \frac{1}{2}u_{k-1}^2}{2\Delta x} = \epsilon \frac{u_{k+1} - 2u_k + u_{k-1}}{\Delta x^2} \quad k = 1, \ldots, K. \tag{20}$$

Here $u_k(t) \approx u(k\Delta x, t)$ and a uniform grid has been assumed.

If we now consider $K = 3$ (not a realistic computation for the PDE, however it serves our purpose of illustrating the dynamics added by the time discretisation) and apply periodic boundary conditions on $x \in [0, 1]$ ($\Delta x = 1/3$) we obtain

$$\begin{array}{rcl} \dot{u} + \frac{3}{4}(v^2 - w^2) & = & \beta(v - 2u + w) \\ \dot{v} + \frac{3}{4}(w^2 - u^2) & = & \beta(w - 2v + u) \\ \dot{w} + \frac{3}{4}(u^2 - v^2) & = & \beta(u - 2w + v) \end{array} \tag{21}$$

where u,v and w represent the three point values and $\beta = 9\epsilon$. A conservation argument ($u + v + w = 1$) can now be used to eliminate w resulting in the system (13). If $\beta = 0$ the system is Hamiltonian ($H(u, v) = -\frac{3}{4}(u + v)(u-1)(v-1)$) with fixed points $(-1, 1)$, $(1, 1)$, $(1, -1)$ and $(1/3, 1/3)$. The Jacobian of (13) is

$$J = \begin{pmatrix} -3\beta + \frac{3}{2}(1 - u - v) & \frac{3}{2}(1 - u) \\ -\frac{3}{2}(1 - v) & -3\beta - \frac{3}{2}(1 - u - v) \end{pmatrix} \tag{22}$$

orbit	eigenvalues	type	eigenvectors
$(1/3, 1/3)$	$-3\beta \pm i\frac{1}{2}\sqrt{3}$	Center $\beta = 0$	
		Stable Spiral $\beta > 0$	
$(-1, 1)$	$\pm 3/2$	Saddle $\beta = 0$	$(1, -1)^T$, $(1, 0)^T$
$(1, 1)$	$\pm 3/2$	Saddle $\beta = 0$	$(1, 0)^T$, $(0, 1)^T$
$(1, -1)$	$\pm 3/2$	Saddle $\beta = 0$	$(0, 1)^T$, $(1, -1)^T$
$(-1, 1)+\boldsymbol{\delta}_1$		Saddle $\beta > 0$	
$(1, 1)+\boldsymbol{\delta}_2$		Saddle $\beta > 0$	
$(1, -1)+\boldsymbol{\delta}_3$		Saddle $\beta > 0$	

Table 4: The dynamics of the Perturbed Hamiltonian system.

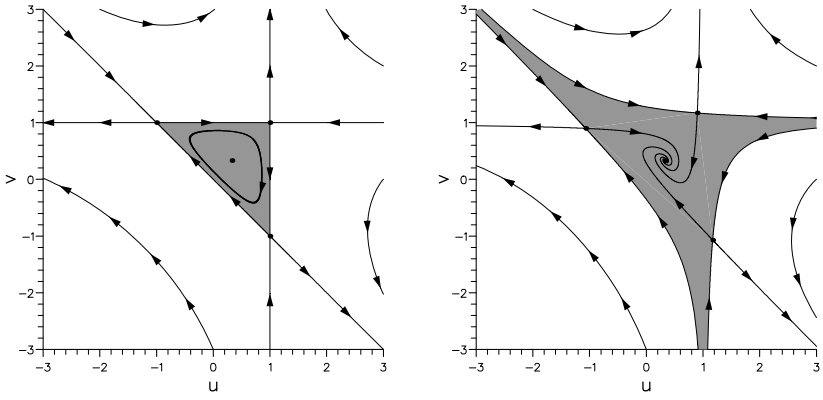

Figure 5: Phase plane for the Perturbed Hamiltonian system, $\beta = 0$ (left) and $\beta > 0$ (right).

and it is easily seen that (for $\beta = 0$) the points $(-1, 1)$, $(1, 1)$ and $(1, -1)$ are saddles whilst $(1/3, 1/3)$ is a center. When $\beta > 0$ (the case in which we are interested) the point $(1/3, 1/3)$ becomes a stable spiral whilst the positions of the saddle are perturbed. The situation is summarised in Table 4 and depicted in Figure 5. Notice how the (shaded) region of non-divergence for $\beta = 0$ stretches to the larger basin of attraction for $\beta > 0$.

In the next section we consider numerical discretisation of these ODE systems and investigate the additional dynamics that the discretisations introduce.

4 The effect of numerical discretisation

The discretisations which we consider are from the Runge-Kutta family of schemes, namely

Euler (RK-1):

$$\mathbf{u}^{n+1} = \mathbf{u}^n + r\mathbf{F}(\mathbf{u}^n) \tag{23}$$

Modified Euler (RK-2):

$$\mathbf{u}^{n+1} = \mathbf{u}^n + r\mathbf{F}(\mathbf{u}^n + \tfrac{1}{2}r\mathbf{F}(\mathbf{u}^n)) \tag{24}$$

Improved Euler (RK-2):

$$\mathbf{u}^{n+1} = \mathbf{u}^n + \tfrac{1}{2}r\{\mathbf{F}(\mathbf{u}^n) + \mathbf{F}(\mathbf{u}^n + r\mathbf{F}(\mathbf{u}^n))\} \tag{25}$$

Heun (RK-3):

$$\begin{aligned} \mathbf{u}^{n+1} &= \mathbf{u}^n + \tfrac{1}{4}(\mathbf{k}_1 + 3\mathbf{k}_3) \\ \\ \mathbf{k}_1 &= r\mathbf{F}(\mathbf{u}^n) \\ \mathbf{k}_2 &= r\mathbf{F}(\mathbf{u}^n + \tfrac{1}{3}\mathbf{k}_1) \\ \mathbf{k}_3 &= r\mathbf{F}(\mathbf{u}^n + \tfrac{2}{3}\mathbf{k}_2) \end{aligned} \tag{26}$$

Kutta (RK-3):

$$\begin{aligned} \mathbf{u}^{n+1} &= \mathbf{u}^n + \tfrac{1}{6}(\mathbf{k}_1 + 4\mathbf{k}_2 + \mathbf{k}_3) \\ \\ \mathbf{k}_1 &= r\mathbf{F}(\mathbf{u}^n) \\ \mathbf{k}_2 &= r\mathbf{F}(\mathbf{u}^n + \tfrac{1}{2}\mathbf{k}_1) \\ \mathbf{k}_3 &= r\mathbf{F}(\mathbf{u}^n - \mathbf{k}_1 + 2\mathbf{k}_2) \end{aligned} \tag{27}$$

RK-4:

$$\begin{aligned} \mathbf{u}^{n+1} &= \mathbf{u}^n + \tfrac{1}{6}(\mathbf{k}_1 + 2\mathbf{k}_2 + 2\mathbf{k}_3 + \mathbf{k}_4) \\ \\ \mathbf{k}_1 &= r\mathbf{F}(\mathbf{u}^n) \\ \mathbf{k}_2 &= r\mathbf{F}(\mathbf{u}^n + \tfrac{1}{2}\mathbf{k}_1) \\ \mathbf{k}_3 &= r\mathbf{F}(\mathbf{u}^n + \tfrac{1}{2}\mathbf{k}_2) \\ \mathbf{k}_4 &= r\mathbf{F}(\mathbf{u}^n + \mathbf{k}_3) \end{aligned} \tag{28}$$

where the numeric identifier after **RK** indicates the order of accuracy of the scheme. Note that the Euler scheme (23) is also a Linear Multistep method and as such will possess only the fixed points of the differential system ([11]). All of the other methods are nonlinear in $\mathbf{F}$ and so will possess spurious fixed points in addition to those of the differential system ([11]).

As is easily appreciated, mathematical analysis of the dynamics of the higher order methods is not practical, even with the aid of algebraic manipulators (e.g. [15, 5, 16]). However some analysis is possible for the lower

order schemes applied to some of our examples. Where rigorous analysis is impractical we have still been able to investigate the dynamics using numerical experiments. For this the NASA Ames Connection Machine CM2 was used which enabled vast numbers (typically 512^2) calculations to be performed in parallel, each calculation identical apart from either initial data or time-step parameter. It was therefore possible to obtain both full bifurcation diagrams in a (r, u) plane and orbits with their basins of attraction in the (u, v) plane. This enabled us to obtain a detailed picture of the dynamical behaviour of the discretisations which would be impossible using scalar or vector machines. Details of the techniques used for detection of the orbits and basins of attraction are given in the Appendix.

The figures presented in this report are of two types. The first type is a full bifurcation diagram where the values of the discrete solution are recorded for fixed r after a certain number (typically 1000) time-steps have first been taken for the trajectories to settle to their asymptotic behaviour. This is repeated for a range of values of r giving the behaviour of the trajectories as r varies. As stated this would give a three dimensional graph $((r, u, v))$ and so for ease of viewing we have taken slices in $v =$ constant planes.

The term "full" in this context indicates that many trajectories for each value of r, corresponding to different initial data, have been taken in order to obtain a complete picture. This is necessary since solutions with different initial conditions will converge to different asymptotic limits; this is occasionally illustrated in our diagrams by the inclusion of basins of attraction, trajectories commencing in a particular basin converging to the fixed point also within that basin. For the bifurcation diagrams the basins must be interpreted as vertical slices since in each calculation r is held fixed. Note also that these basins may often be fragmented and so separate regions (viewed as a vertical slice) with the same shading correspond to the same basin and attractor. Such basins are best illustrated using colour, unfortunately it is not possible to include colour pictures in this report and so the grayscale representations are only included when needed to illustrate particular points.

The second type of diagram depicts the asymptotic orbits of the solution for fixed r in the (u, v) plane. Again different initial data will converge (or not) to different asymptotic behaviour and so basins of attraction are again used, where necessary, to illustrate this. For these diagrams the basins should be interpreted in a true two dimensional manner and not as vertical slices as for the bifurcation diagrams.

We consider the problems (10)–(13) in turn, presenting an investigation of the dynamics of the discretisations both by numerical experiment, and where practical by mathematical analysis. Of course the total number of combinations (24 for each value of β) is too large to contemplate practically, especially since each case necessitates a number of numerical experiments to adequately sample the three dimensional space (r, u, v). We have therefore

been very selective in the results presented here, but even so the prescence and nature of spurious dynamical behaviour is evident.

4.1 The Predator Prey equations

Due to consistency, the fixed points of the ODEs will also be fixed points of the Runge-Kutta schemes which we are considering. However, the stability (and type) of these essential fixed points of the schemes will depend on the parameter r, the stability condition for a k-th order Runge-Kutta method being ([14]) $|\mu| < 1$ where

$$\mu = 1 + r\lambda + \cdots + \frac{r^k \lambda^k}{k!} \tag{29}$$

and λ ranges over the eigenvalues of the Jacobian J of the system of ODEs. (This expression arises from the fact that the scheme is a k-th order approximation to the ODEs.) It is easily verified that if $\Re e(\lambda) > 0$ then $|\mu| > 1$ and so unstable fixed points of the ODEs will not be stable fixed points of the scheme, although as we shall see their type may change.

For the Euler scheme (23) the stability polynomial (29) is just $\mu = 1 + r\lambda$ and so we can use the eigenvalues from Table 1 to obtain the stability and type of each of the fixed points. For illustrative purposes we shall give the details for this simple case, however in general we shall just state the results, the analysis being straight forward (if tedious). We have therefore, for the fixed points of the Euler scheme applied to the Predator Prey equations

$(0,0)$: $\mu_1 = 1 - 3r$, $\mu_2 = 1 - 2.1r$
Stable node $r \in (0, \frac{2}{3})$,
Saddle $r \in (\frac{2}{3}, \frac{2}{2.1} = 0.\dot{9}52380\dot{9})$
Unstable node $r > 0.\dot{9}52380\dot{9}$

$(1,0)$: $\mu_1 = 1 - 1.1r$, $\mu_2 = 1 + 2r$
Saddle $r \in (0, 1.81\dot{8}\dot{1})$
Unstable node $r > 1.81\dot{8}\dot{1}$

$(3,0)$: $\mu_1 = 1 - 6r$, $\mu_2 = 1 + .9r$
Saddle $r \in (0, \frac{1}{3})$
Unstable node $r > \frac{1}{3}$

$(2.1, 1.98)$: $\mu = 1 + r(-0.21 \pm i\sqrt{2.0349})$,
$|\mu|^2 = 1 - 0.42r + 2.079r^2$
Stable spiral $r \in (0, 0.20\dot{2}\dot{0})$,
Unstable spiral $r > 0.20\dot{2}\dot{0}$

As can be seen, not only is the stability of the fixed points dependent on the parameter r but also their type. As the fixed point $(0,0)$ becomes unstable at $r = \frac{2}{3}$ the eigenvalue μ_1 of the scheme is -1 and so we might expect a period doubling flip bifurcation to occur. This is bourne out by the bifurcation diagram of Figure 6 which depicts a slice through the three dimensional bifurcation diagram on the plane $v = 0$. The period 2 orbit lies in the $v = 0$ plane since the eigenvector corresponding to μ_1 (and λ_1) is $(1,0)^T$.

Figure 6 shows an interesting consequence of our technique for locating fixed points (see the Appendix for details), namely that since the stable eigendirection of the saddle at $(3,0)$ lies in the $v = 0$ plane it has been detected and represented on the bifurcation diagram. Notice that when this saddle becomes an unstable node at $r = \frac{1}{3}$ again $\mu_1 = -1$ and so period doubling is observed. Figures 7 – 9 illustrate orbits of the solution in the (u, v) plane for three different values of r. Notice that in these pictures the saddle does not appear whereas the fixed point (and its bifurcation) does.

When the spiral becomes unstable the eigenvalues are complex and so a Hopf bifurcation occurs giving rise to a limit cycle as depicted in Figures 10 and 8. Whereas bifurcation to a period two solution is readily detectable in numerical calculations, bifurcation to a limit cycle will not be so obvious, especially in the vicinity of the bifurcation (in the parameter r) and in higher dimensional problems. Indeed the phenomenon of an artificial time iteration to steady-state, of a large system formed by spatial discretisation, which gets near to convergence before the residuals "plateau out" could actually be the result of a limit cycle.

Finally note that although no spurious fixed points are generated by the Euler scheme higher order period solutions, stable or unstable, are possible. Such spurious solutions can have a drastic effect on the basins of attraction of the true fixed points as is illustrated in Figure 11 where it can be seen that the basins for $(0,0)$ and $(2.1, 1.98)$ which extend to $\pm\infty$ for the ODEs are severely truncated, as well as becoming segmented. One period 2 solution of the Euler scheme applied to these equations is given by

$$\left(\tfrac{3}{2} \pm \tfrac{1}{2}\sqrt{9 + 4/r}, 0\right) \tag{30}$$

which for $r = 0.1$, the case for Figure 11, take the values $(-2, 0)$ and $(5, 0)$ which both lie on the boundaries of the truncated basins of attraction. This illustration should cause particular concern since it occurs at a value of r which is well below the linearised stability limit of both fixed points.

The linearised stability regions for the two stable fixed points are summarised for all of the Runge-Kutta methods we are considering in Table 5. We will only consider one other of them in detail here, namely the Modified

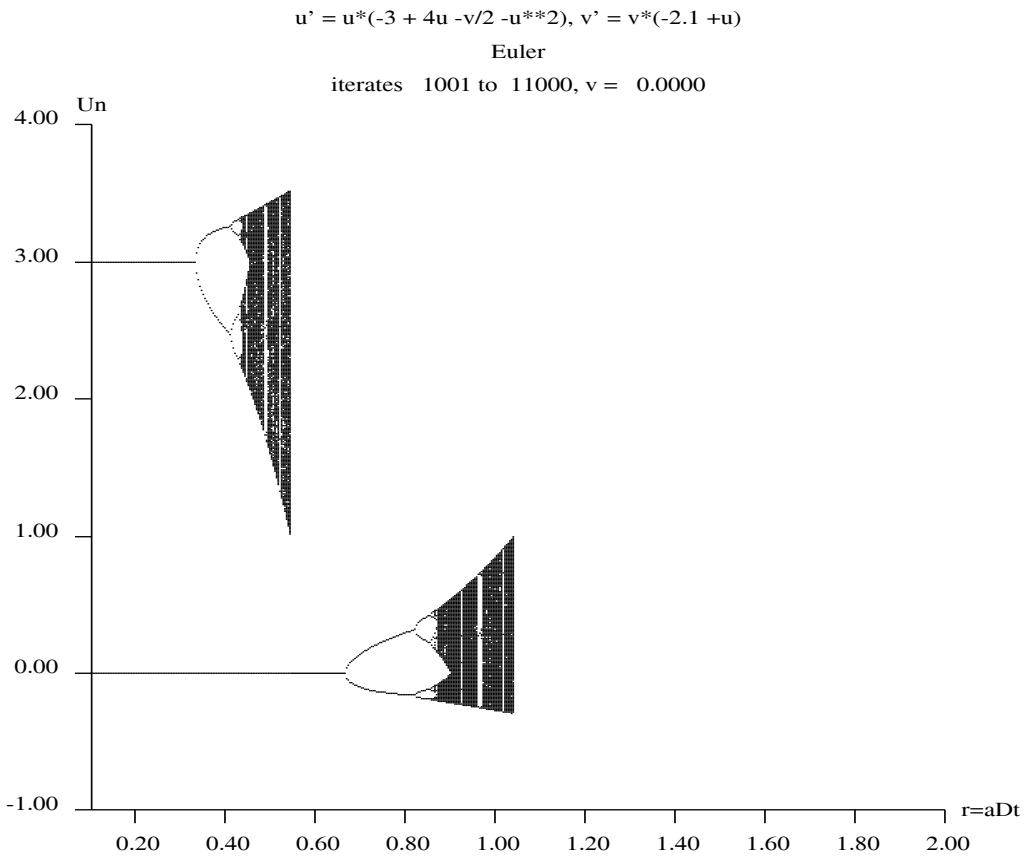

Figure 6: Bifurcation diagram for the Predator Prey equations using the Euler scheme.

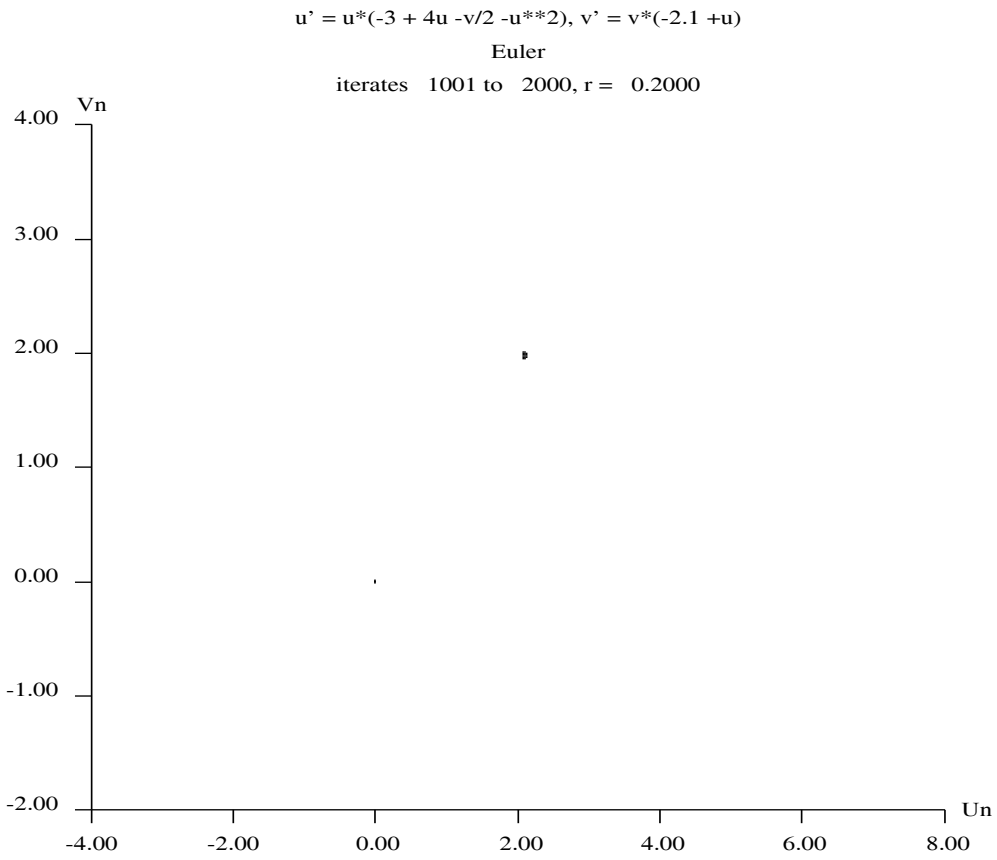

Figure 7: Phase orbits for the Predator Prey equations using the Euler scheme.

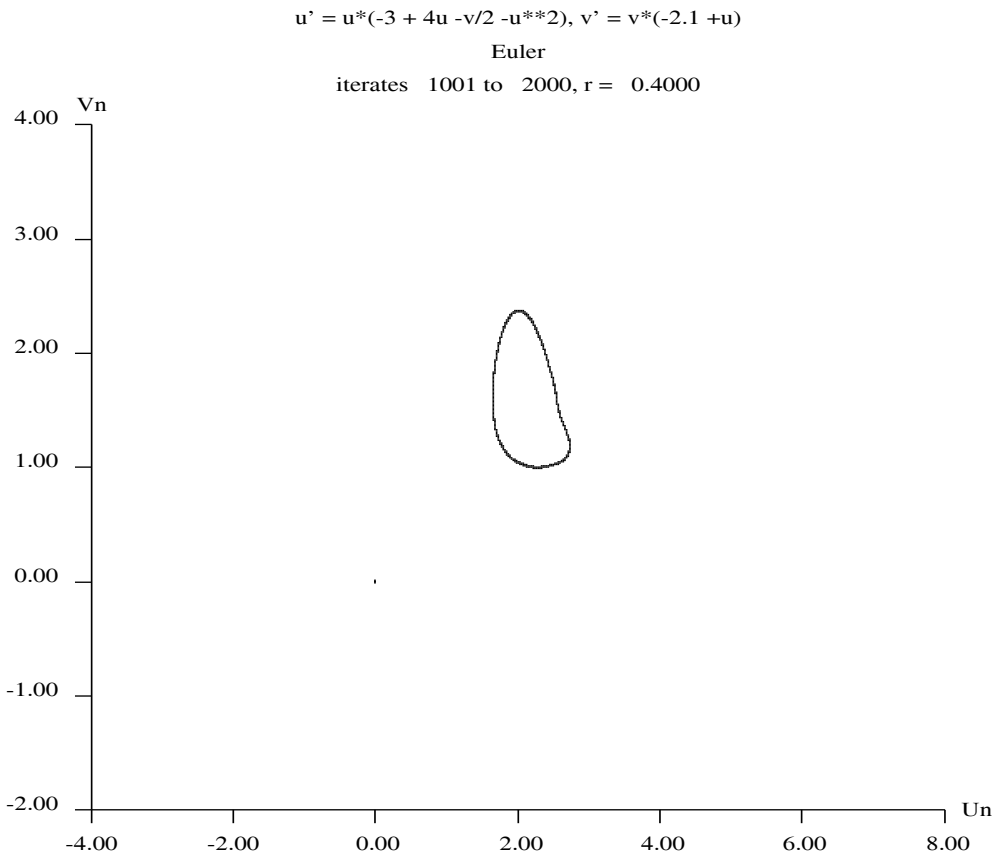

Figure 8: Phase orbits for the Predator Prey equations using the Euler scheme $r = 0.4$.

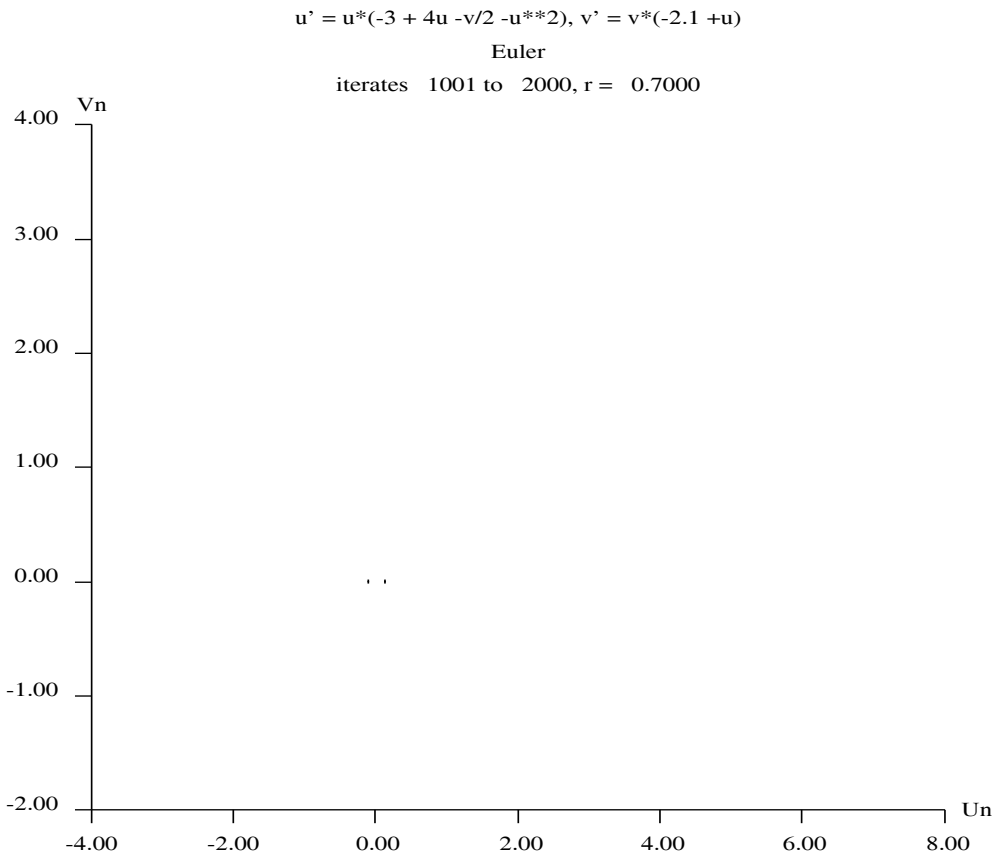

Figure 9: Phase orbits for the Predator Prey equations using the Euler scheme $r = 0.7$.

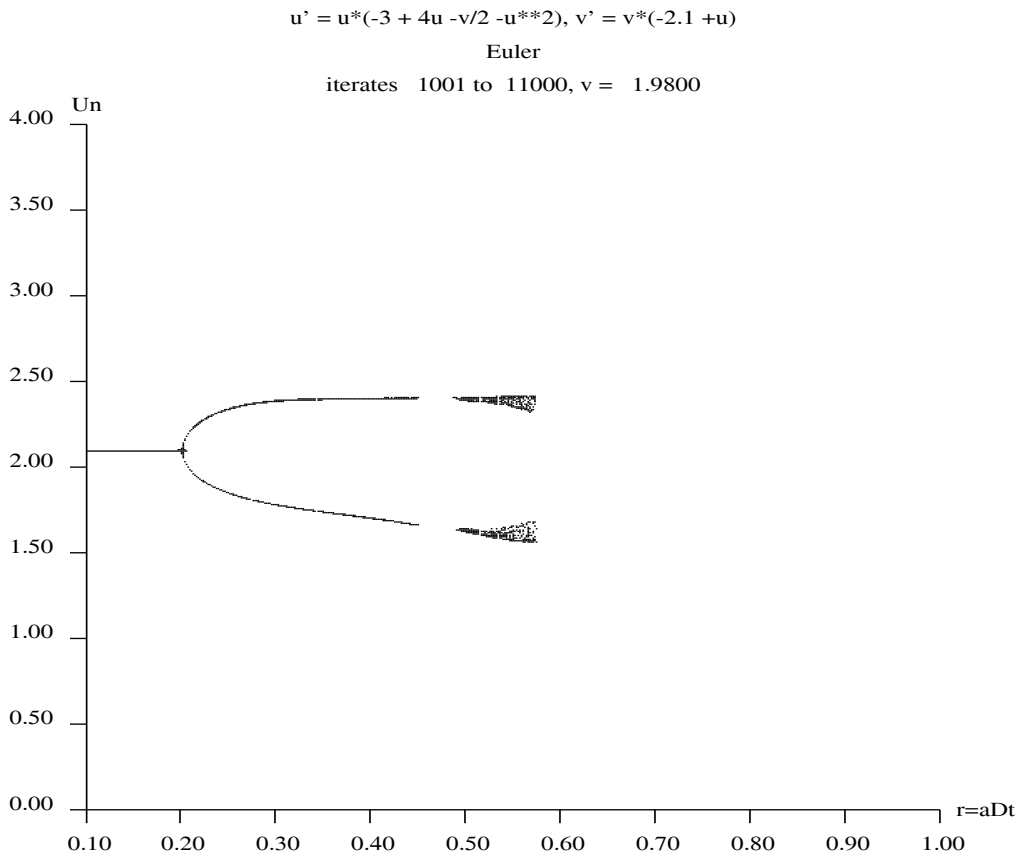

Figure 10: Bifurcation diagram for the Predator Prey equations using the Euler scheme.

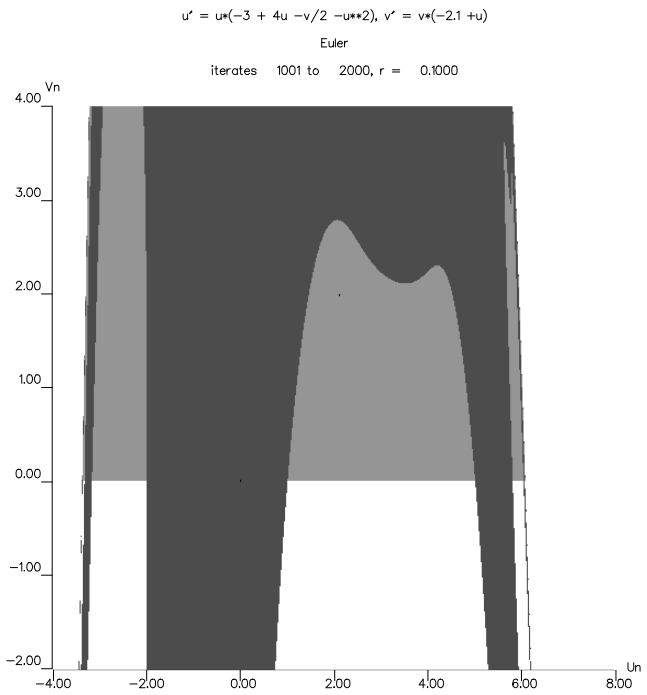

Figure 11: Basins of attraction for the Predator Prey equations using the Euler scheme.

	$(0,0)$	$(2.1, 1.98)$
RK-1	$r \in (0, \frac{2}{3})$	$r \in (0, 0.2020)$
RK-2	$r \in (0, \frac{2}{3})$	$r \in (0, 0.848102)$
RK-3	$r \in (0, 0.837581)$	$r \in (0, 1.57240)$
RK-4	$r \in (0, 0.928431)$	$r \in (0, 2.05281)$

Table 5: Linearised stability regions for the Predator Prey equations.

Key	$\mathbf{u}_S$	Type	Stability[1]	$\mathbf{u}_E$
1	$(2 - \sqrt{1 + 2/r}, 0)$	Saddle $\rightarrow$ Node	$r \in (\frac{2}{3}, 1.10704)$	$(0,0)$
2	$(2 + \sqrt{1 + 2/r}, 0)$	Saddle $\rightarrow$ Node		$(0,0)$
3	$(\frac{3}{2} - \frac{1}{2}\sqrt{9 + 8/r}, 0)$	Node $\rightarrow$ Saddle	$r \in (0, 0.418871)$	$(1,0)$
4	$(\frac{3}{2} + \frac{1}{2}\sqrt{9 + 8/r}, 0)$	Node $\rightarrow$ Saddle	$r \in (0, 0.31502)$	$(1,0)$
5	$(\frac{1}{2} - \frac{1}{2}\sqrt{1 + 8/r}, 0)$	Node $\rightarrow$ Saddle		$(3,0)$
6	$(\frac{1}{2} + \frac{1}{2}\sqrt{1 + 8/r}, 0)$	Node $\rightarrow$ Saddle		$(3,0)$

Table 6: Spurious fixed points in the $v = 0$ plane for Modified Euler.

Euler scheme (24) which we will see has stable spurious fixed points occurring below the linearised stability limits of the essential fixed points.

From the form (24) of the Modified Euler scheme it is easily seen that as well as the essential fixed points $\mathbf{u}_E$ of the ODEs, any other value $\mathbf{u}_S$ satisfying

$$\mathbf{u}_S + \tfrac{1}{2} r \mathbf{F}(\mathbf{u}_S) = \mathbf{u}_E \tag{31}$$

will also be a fixed point of the scheme. We refer to these additional fixed points as spurious fixed points. Note that the $\mathbf{u}_E$ on the right-hand side of (31) encompasses both stable and unstable fixed points of the ODE and so for the Predator Prey equations (since $\mathbf{F}$ contains cubes) there are up to twelve (real) spurious steady states, 3 for each essential fixed point. In fact there are six such spurious steady states which lie in the $v = 0$ plane, all of them occurring below the linearised stability limits of the essential fixed points, although not all are stable there. These six are summarised in Table 6 and shown in the bifurcation diagram of Figure 12. Notice again how the saddle at $(3, 0)$ appears since its stable eigen-direction is in the $v = 0$ plane.

Notice how the spurious fixed point 1 bifurcates transcritically from the

[1]Since these are spurious roots it is the eigenvalues of the matrix $I + rJ(\mathbf{u}_E) + \frac{1}{2}r^2 J(\mathbf{u}_S)J(\mathbf{u}_E)$ which must be examined for stability and not μ given by (29).

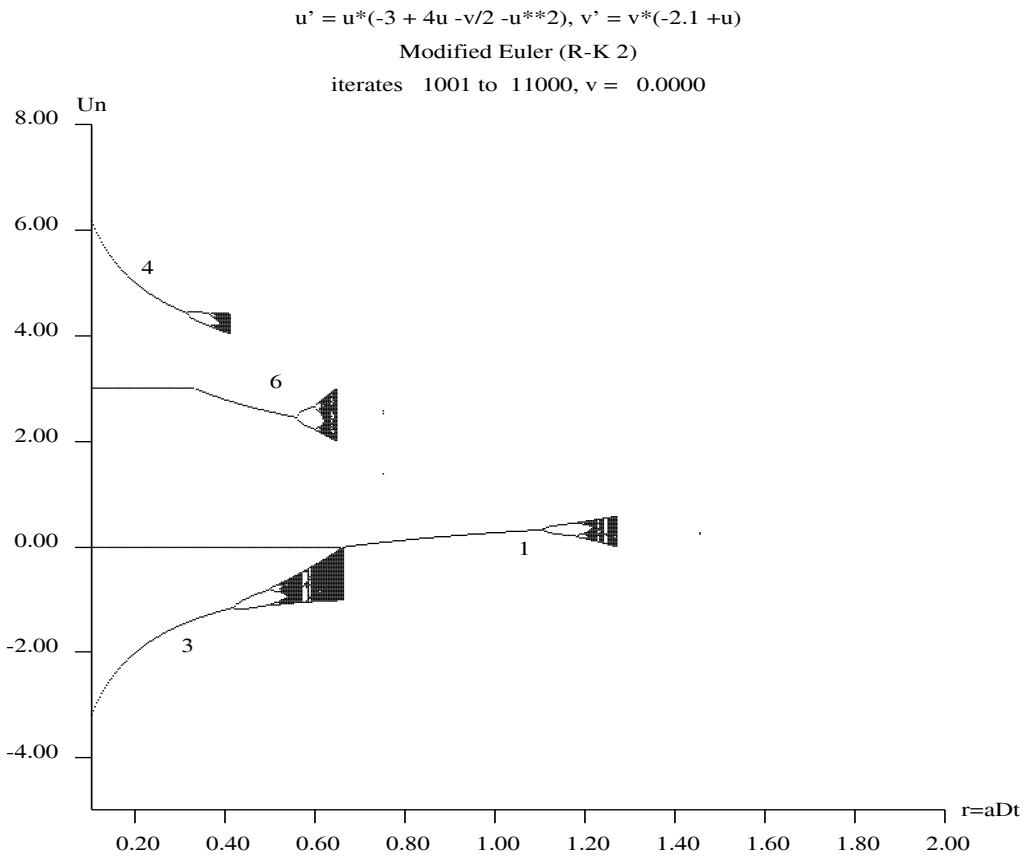

Figure 12: Bifurcation diagram for The Predator Prey equations using the Modified Euler scheme.

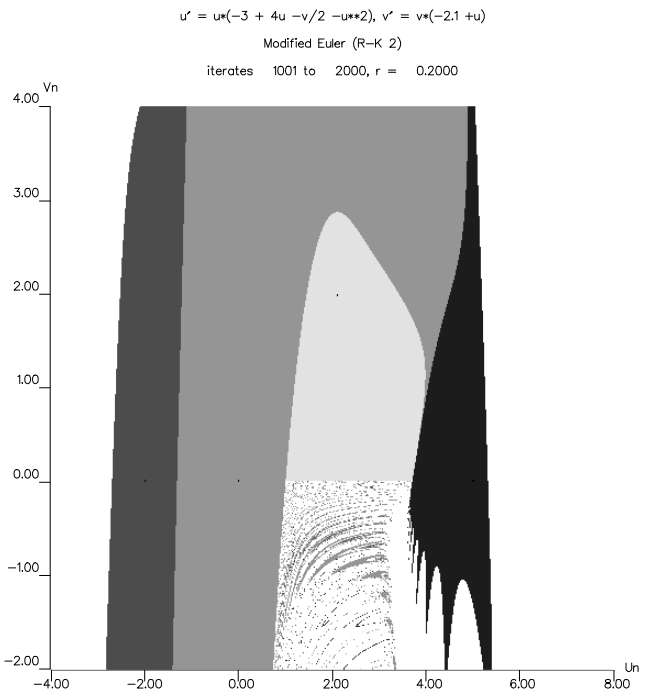

Figure 13: Spurious fixed points and their basins of attraction for the Predator Prey equations using the Modified Euler scheme.

essential fixed point $(0, 0)$. Such a bifurcation could easily go unnoticed in numerical calculations, indeed in Figures 14 and 15 the fixed point shown near the origin is in fact not at the origin where the essential fixed point should be. Figure 13 illustrates the spurious fixed points together with their basins of attraction and Figure 15 shows the limit cycle obtained after the spiral at $(2.1, 1.98)$ becomes unstable. Notice the edge of another (spurious) orbit in the vicinity of $(0, -4)$.

Finally for the Predator Prey equations, although we do not investigate them analytically the bifurcation diagrams in the $v = 0$ plane for the remaining schemes are given in Figures 16 – 19.

We remark that due to a result by Humphries [10] spurious fixed points of Runge-Kutta schemes applied to locally Lipschitz $\mathbf{F}$ (which is the case for the Predator Prey equations) can only exist for $r \to 0$ if they become unbounded

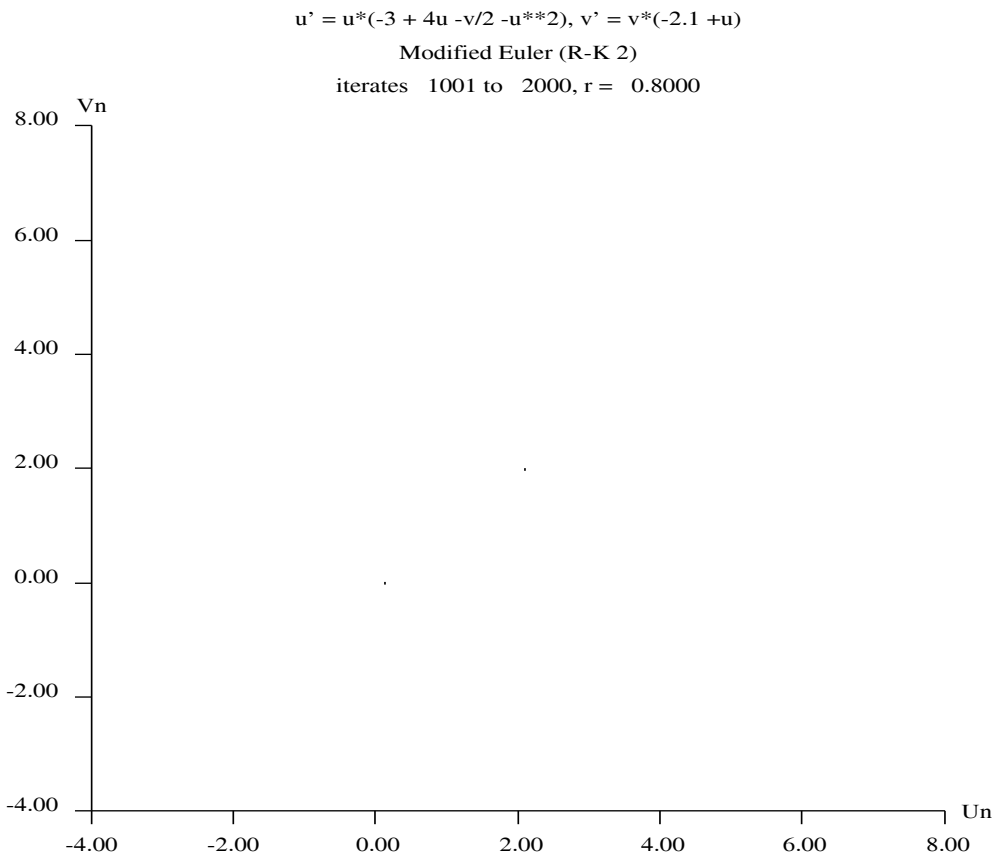

Figure 14: Incorrect (spurious) fixed point near origin for the Predator Prey equations using the Modified Euler scheme.

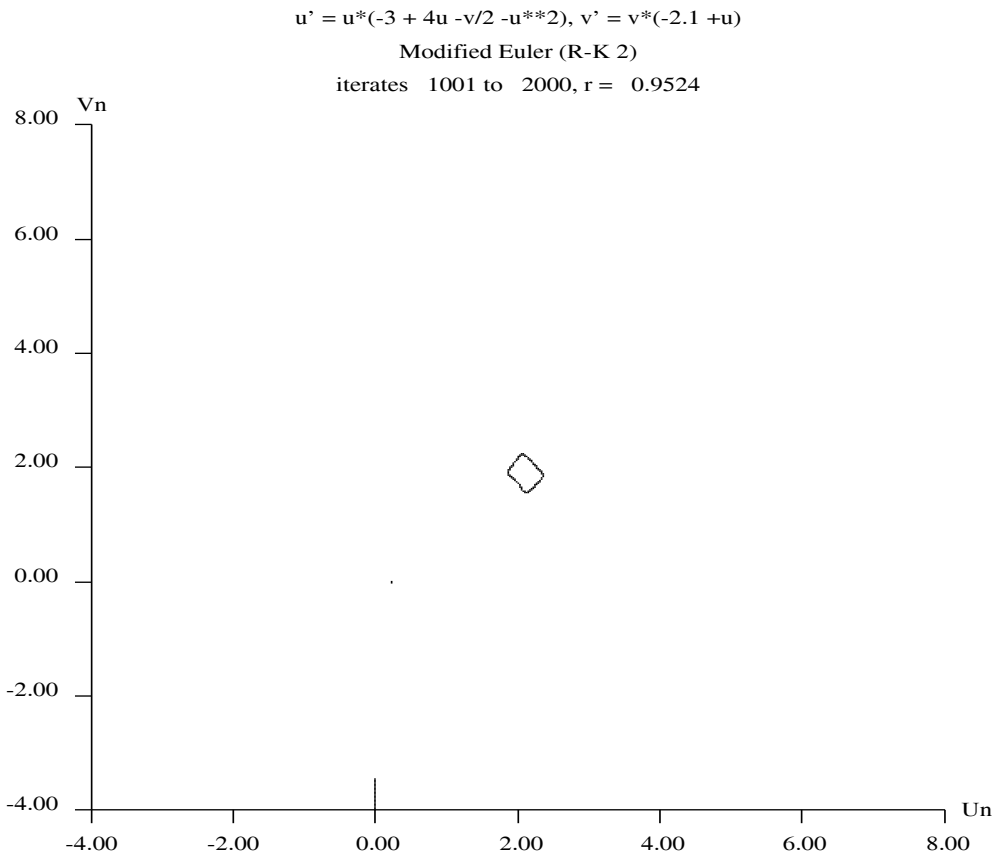

Figure 15: Spurious limit cycle for the Predator Prey equations using the Modified Euler Scheme.

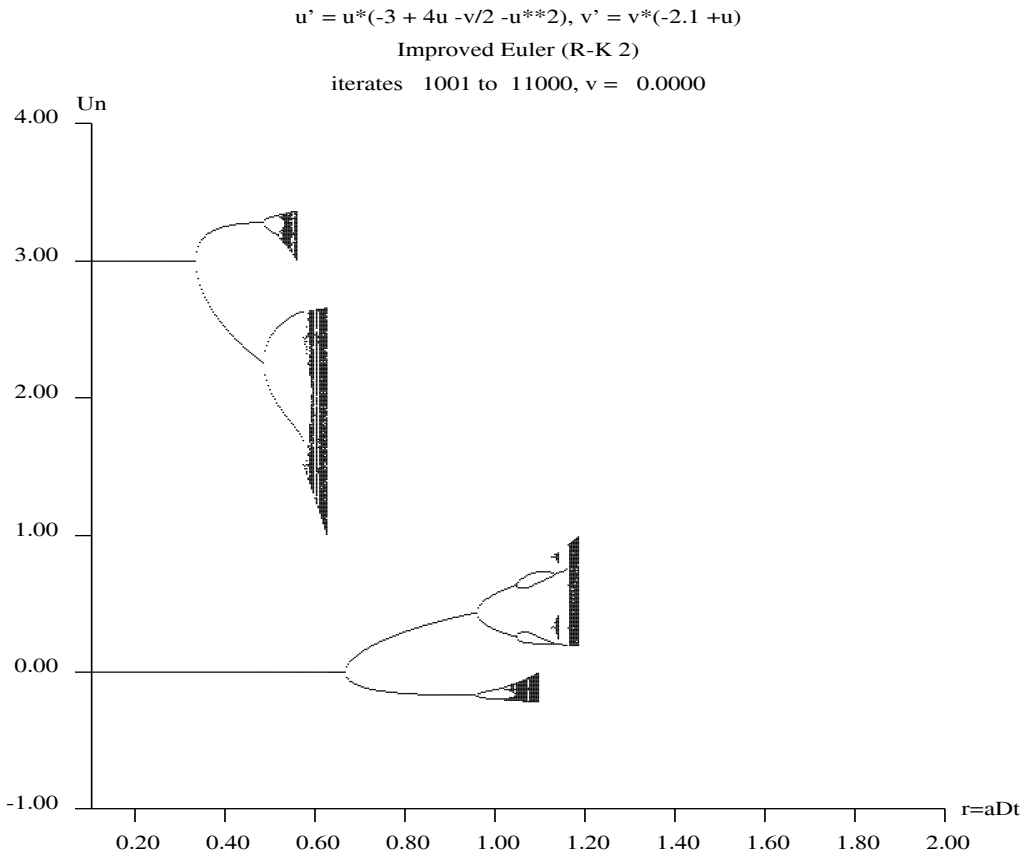

Figure 16: Bifurcation diagram for the Predator Prey equations using the Improved Euler Scheme.

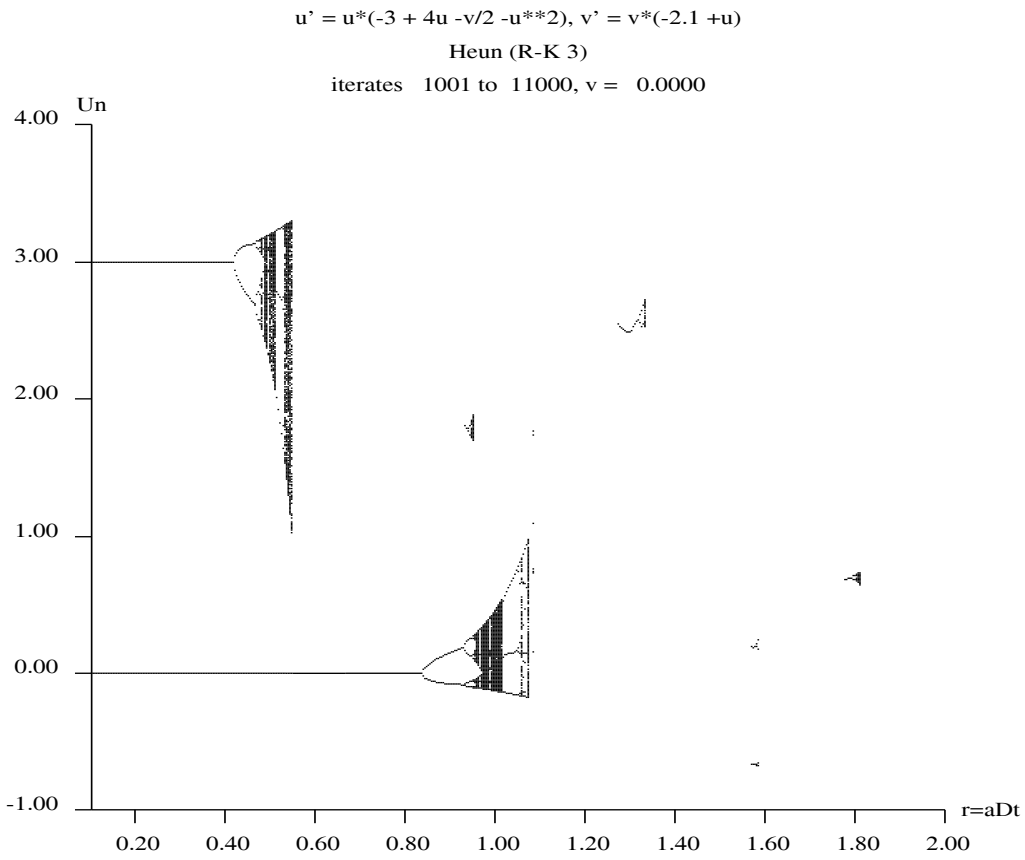

Figure 17: Bifurcation diagram for the Predator Prey equations using the Heun scheme.

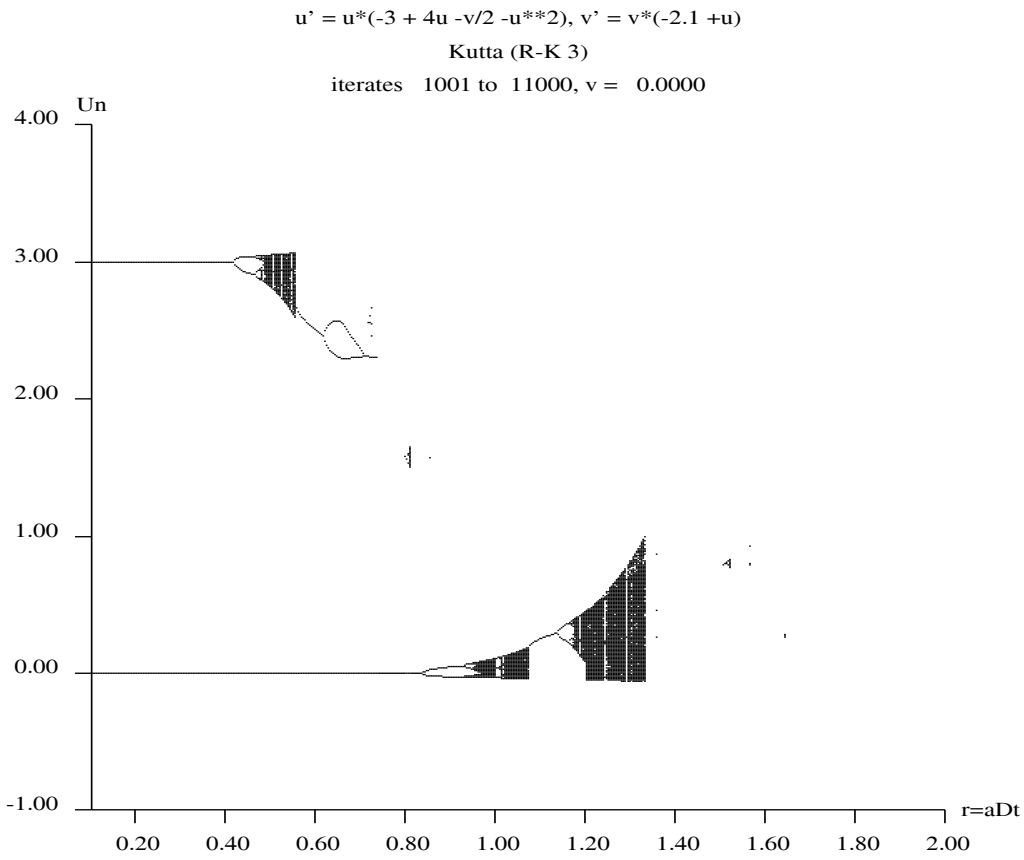

Figure 18: Bifurcation diagram for the Predator Prey equations using the Kutta scheme.

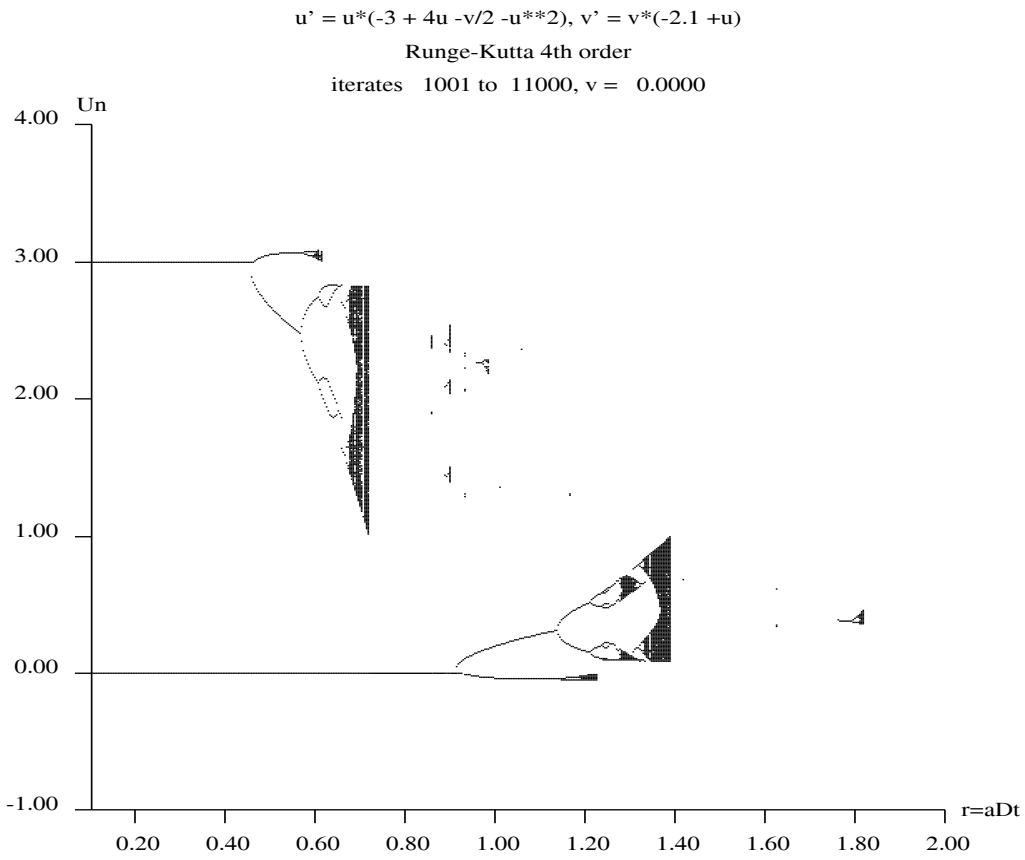

Figure 19: Bifurcation diagram for the Predator Prey equations using the RK-4 scheme.

which is obviously the case here due to the appearance of the reciprocal of r. For globally Lipschitz $\mathbf{F}$ Humphries results states that spurious fixed points can not exist for arbitrarily small r, again this is bourne out by our results for the Damped Pendulum equation.

4.2 The Damped Pendulum equation

If we apply the Euler scheme (23) to the Damped Pendulum equation (11) we find, as expected, that the saddles at $((2m+1)\pi, 0)$ remain saddles and that the type of the fixed points (when stable) at $(m\pi, 0)$ are as for the ODE, spirals for $\beta < 2$ and nodes for $\beta > 2$. Further more it is easy to obtain the linearised stability regions for these fixed points as being

$$r \in (0, \beta) \qquad \beta < 2 \tag{32}$$

and

$$r \in (0, \beta - \sqrt{\beta^2 - 4}) \qquad \beta > 2. \tag{33}$$

We shall concentrate on the case $\beta < 2$ and look for period two solutions.

Period two solutions of the Euler scheme must satisfy

$$\mathbf{F}(\mathbf{u}) + \mathbf{F}(\mathbf{u} + r\mathbf{F}(\mathbf{u})) = 0, \qquad \mathbf{F}(\mathbf{u}) \neq 0 \tag{34}$$

which for the Damped Pendulum equation becomes, after some manipulation,

$$\begin{cases} (2 - r\beta)v &= r\sin(u) \\ \sin(u)(1 + \cos(rv)) &= -\cos(u)\sin(rv) \end{cases}. \tag{35}$$

Eliminating u we obtain

$$(2 - r\beta)v = r\sqrt{\frac{1 - \cos^2(rv)}{2}} \tag{36}$$

and treating both sides as functions of a new variable rv we see, by considering derivatives at the origin, that solutions of this equation will exist for

$$-\tfrac{1}{2}r^2 < 2 - r\beta < \tfrac{1}{2}r^2. \tag{37}$$

It is then easily seen that such solutions exist for $r < \beta$, i.e. below the linearised stability limit of the fixed points.

For the Predator Prey equations solved by the Euler scheme we presented formulae for some period two solutions below the linerised stability limit, but these were unstable. However, as can be seen from Figure 20, for the Damped Pendulum these subcritical period two solutions can be stable, the checkerboard shading of the figure indicating the basins of attraction both of the period two solutions and of the true fixed points. Nearer the linearised

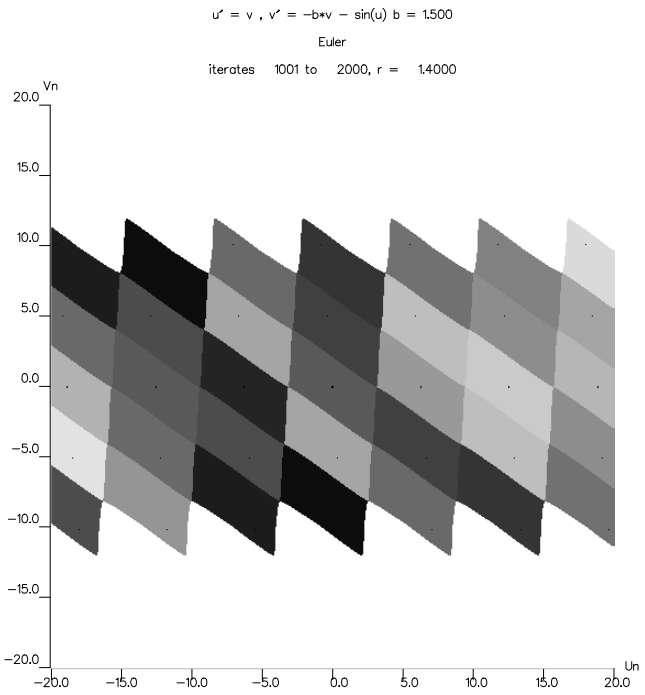

Figure 20: Subcritical period two solutions and their basins of attraction for the Damped Pendulum using the Euler scheme.

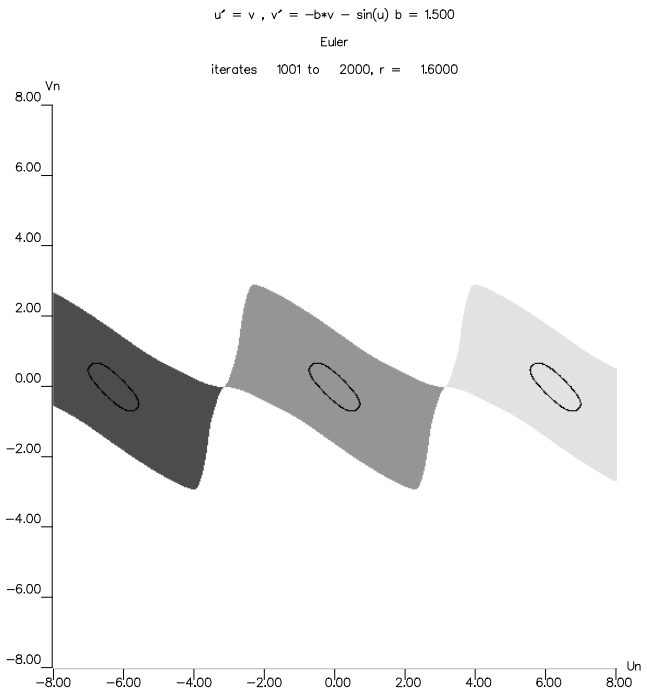

Figure 21: Spurious limit cycles and their basins of attraction for the Damped Pendulum using the Euler scheme.

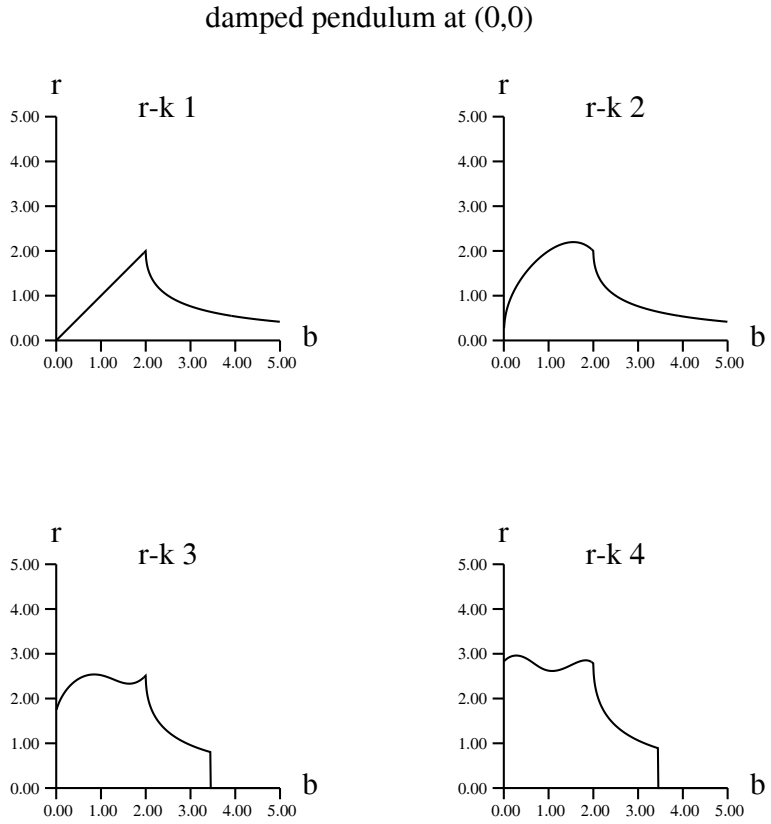

Figure 22: Stability regions for the Damped Pendulum.

stability limit these period two orbits become unstable and the fixed points (spirals) bifurcate into limit cycles as illustrated in Figure 21.

Although some analysis is still possible for the second order Runge-Kutta schemes we do not present it here since it is not enlightening in itself. However what analysis we have been able to perform has agreed well with our numerical computations. The stability regions of the schemes are shown in Figure 22 and Figures 23 and 24 illustrate spurious subcritical features of the Modified Euler and RK-4 schemes respectively. For the Modified Euler scheme spurious fixed points are present, whilst for the fourth order Runge-Kutta scheme it is period four solutions which have caused the restriction of the basins of attraction of the essential fixed points.

For our remaining two examples, the Dissipative Complex system and The Perturbed Hamiltonian we present only numerical results, mathematical analysis not being practical.

Figure 23: Spurious subcritical fixed points for the Damped Pendulum using the Modified Euler scheme.

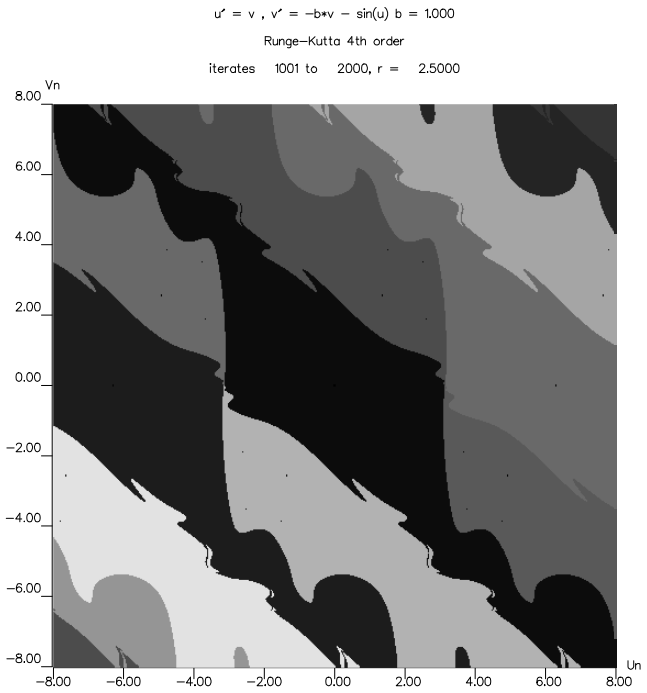

Figure 24: Subcritical period 4 solutions for the Damped Pendulum using the Modified Euler scheme.

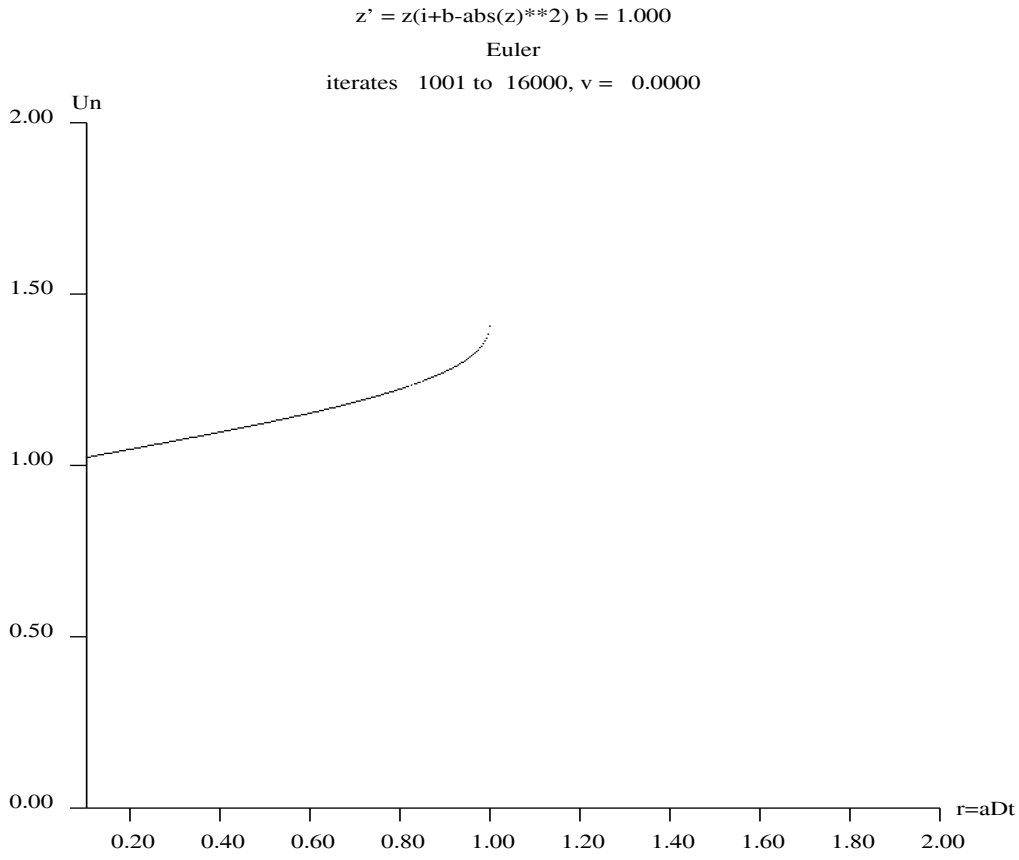

Figure 25: Bifurcation diagram of limit cycle for the Dissipative Complex equation produced by the Euler scheme.

4.3 The Dissipative Complex equation

We consider only the case $\beta > 0$ where the ODE has a limit cycle $|z| = \sqrt{\beta}$. Figures 25 – 30 illustrate the unreliability of trying to compute a true limit cycle with any sizable r. This should not be surprising since the schemes only give an $O(r^k)$ approximation to the solution trajectories, and since the limit cycle is not a fixed point we would expect inaccuracies to be introduced. However, it would be easy to forget this presented a numerical solution which had the qualitative features expected.

4.4 The Perturbed Hamiltonian equation

For this example we present just one illustration using the Kutta scheme to demonstrate how subcritical spurious solutions can occur and affect the

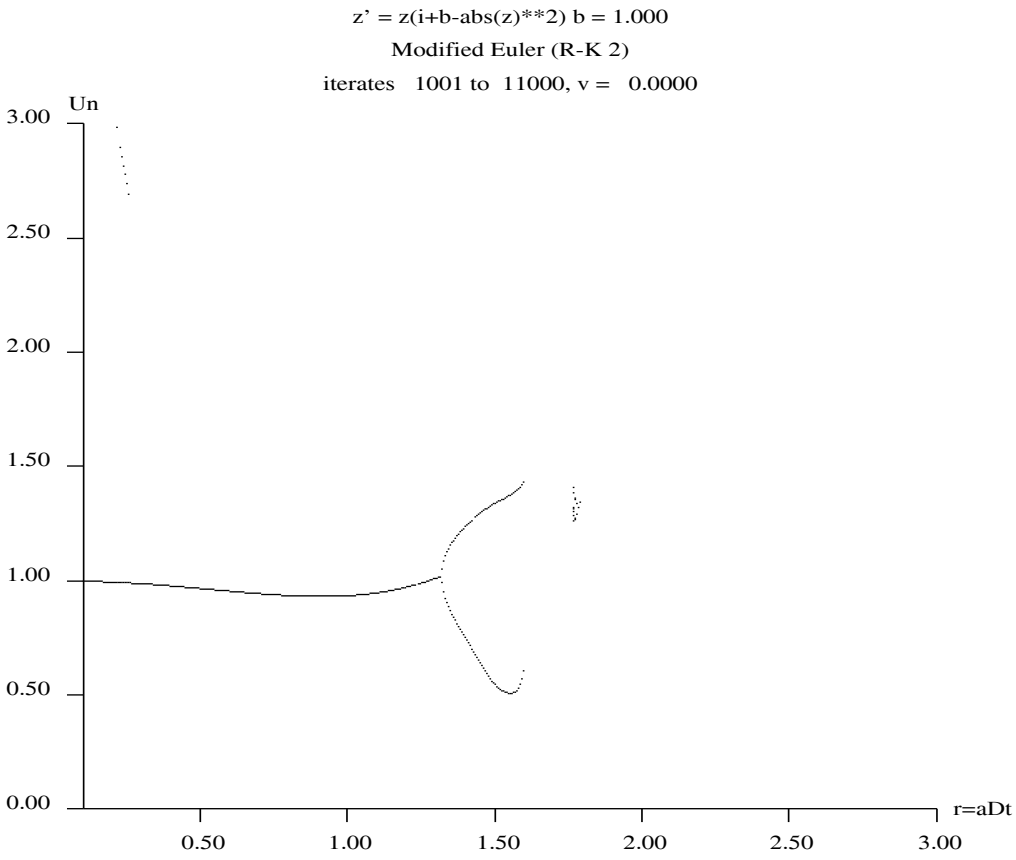

Figure 26: Bifurcation diagram of limit cycle for the Dissipative Complex equation produced by the Modified Euler scheme.

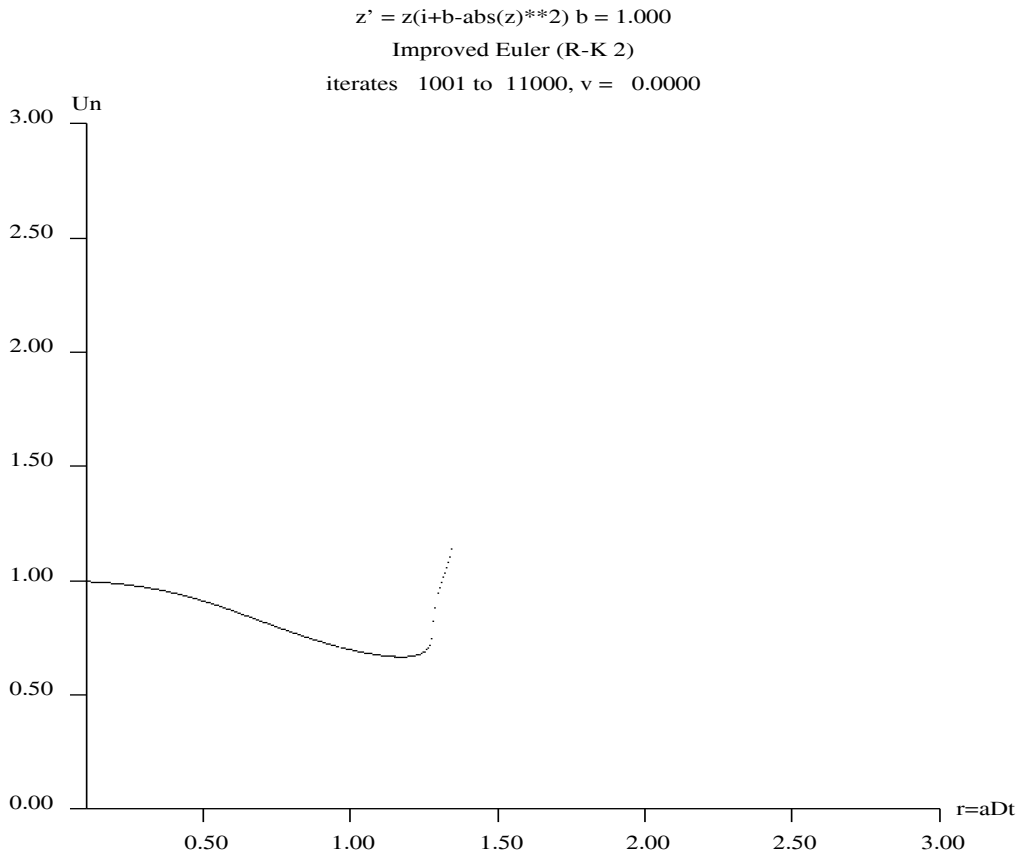

Figure 27: Bifurcation diagram of limit cycle for the Dissipative Complex equation produced by the Improved Euler scheme.

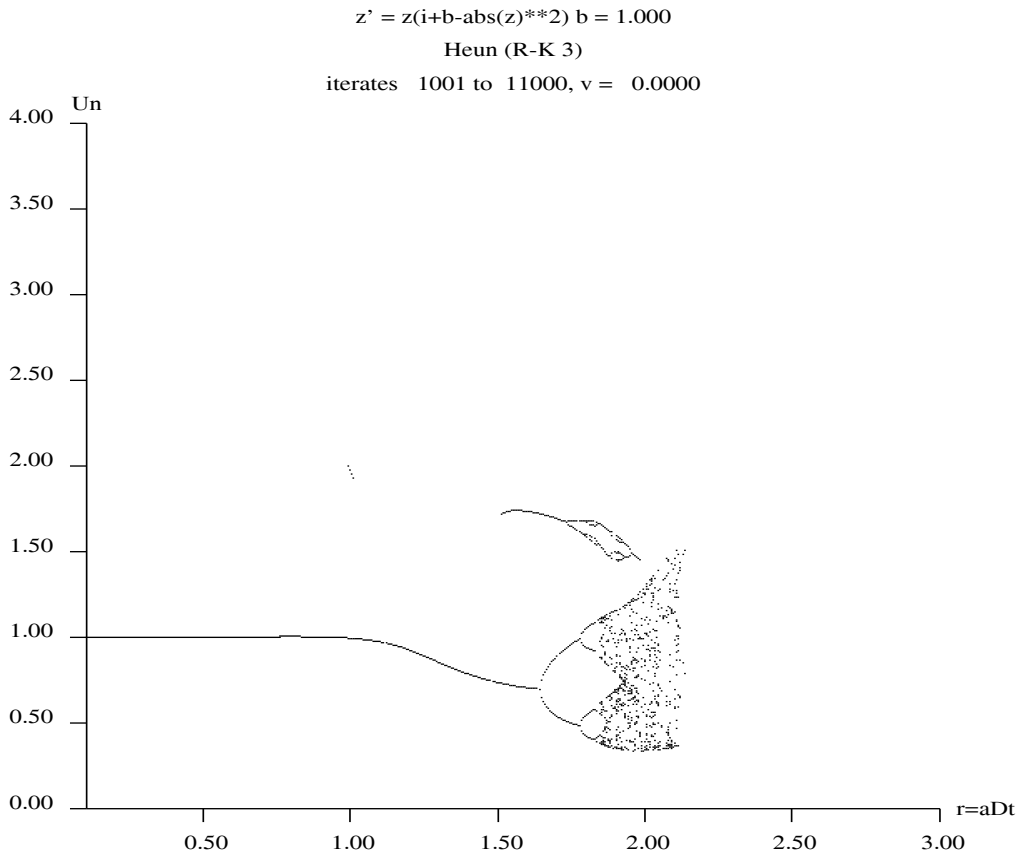

Figure 28: Bifurcation diagram of limit cycle for the Dissipative Complex equation produced by the Heun scheme.

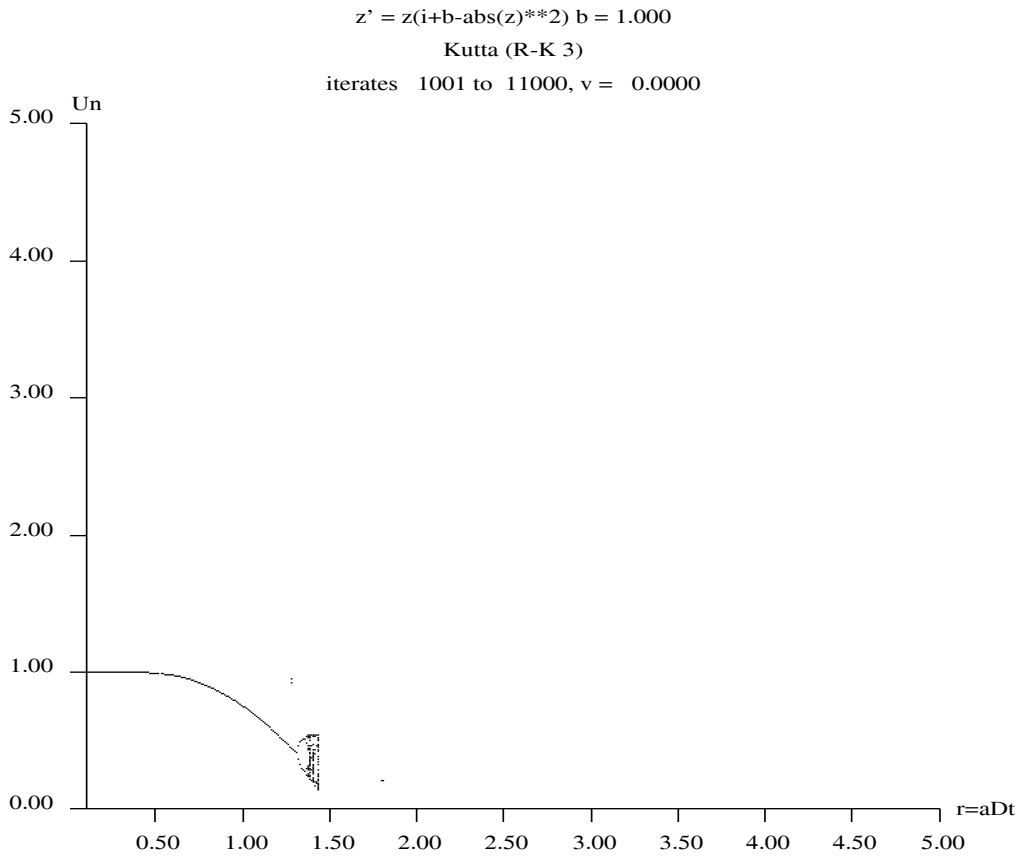

Figure 29: Bifurcation diagram of limit cycle for the Dissipative Complex equation produced by the Kutta scheme.

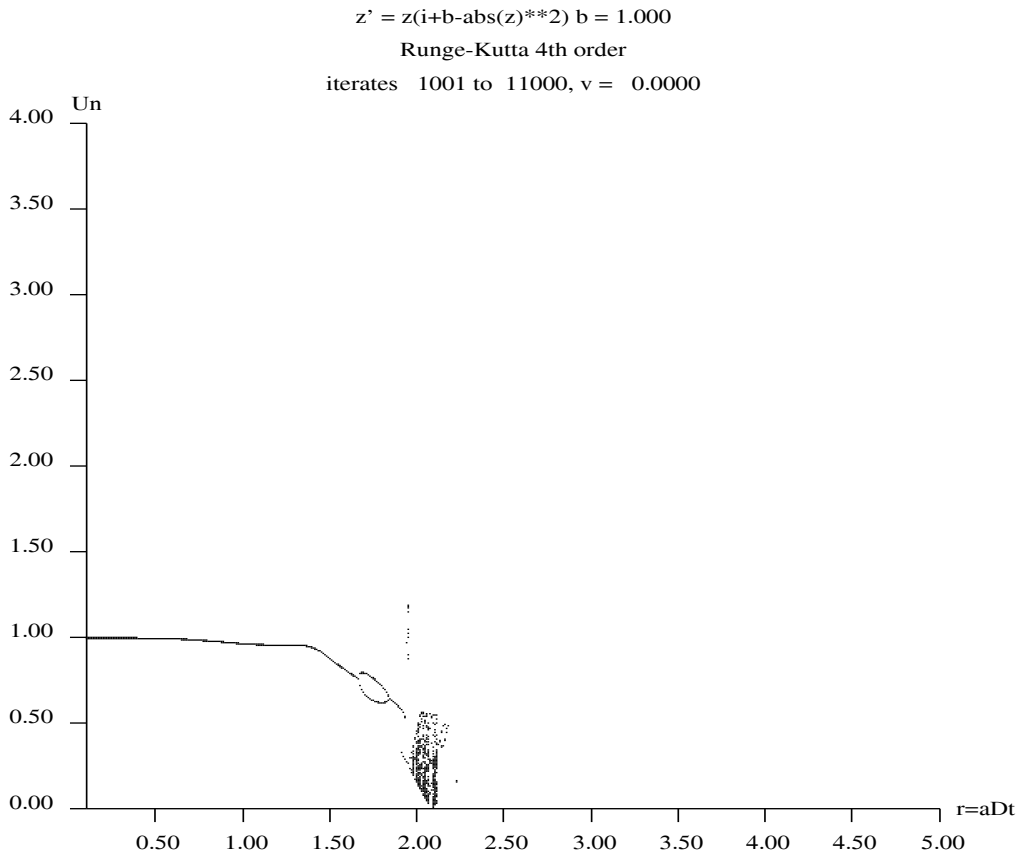

Figure 30: Bifurcation diagram of limit cycle for the Dissipative Complex equation produced by the RK-4 scheme.

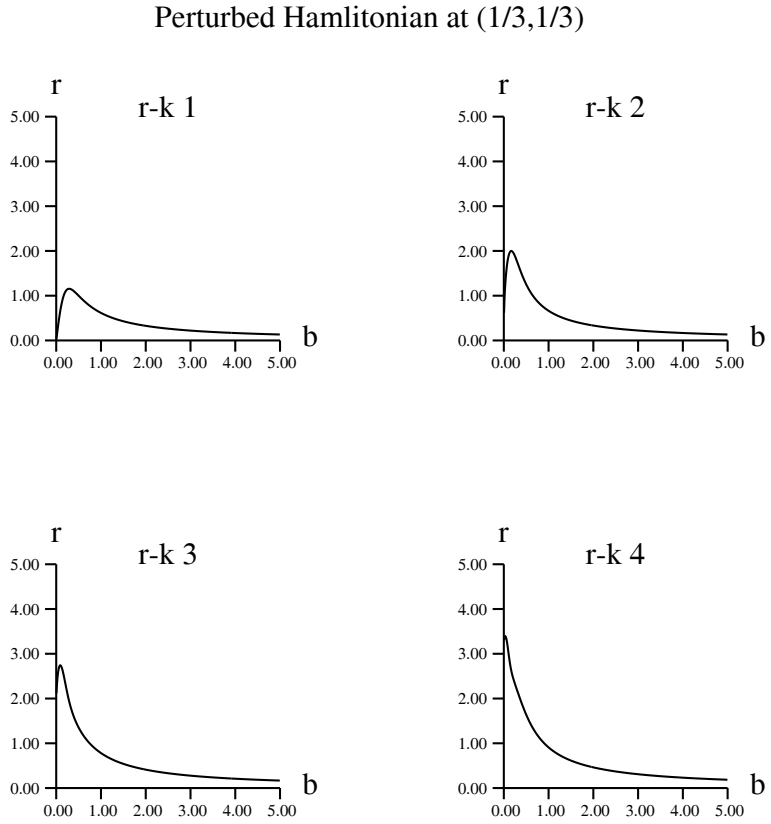

Figure 31: Stability regions for the Perturbed Hamiltonian.

basins of attraction of the true fixed point. This is shown in Figures 32 and 33 with the stability regions being given in Figure 31. We recall that this example may be constructed by a crude approximation to a PDE and so this serves as an indication that problems of spurious dynamical behaviour will arise for the numerical solution of PDEs as well as ODEs.

5 Summary

In the preceding section we have illustrated a number of important ways in which the dynamics of a numerical discretisation of a 2×2 first-order autonomous nonlinear system of ODEs can differ from the system itself. Together with their implications for general systems, including those approximating PDEs these are:

Figure 32: Section of bifurcation diagram for the Perturbed Hamiltonian using the Kutta scheme.

Figure 33: Spurious subcritical behaviour for the Perturbed Hamiltonian using the Kutta scheme.

- Spurious fixed points may be present both below and bifurcating from the linearised stablity limit of the essential fixed point of interest. In the former case the spuriousness of the limit point may not be recognised in complicated stituations and in the latter case the vicinity of the spurious limit point to the (now unstable) true limit point is likely to hide the misplacement in even simple cases.

- Stable and unstable spurious fixed points and higher order orbits drastically affect the basins of attraction of the essential fixed points of the ODEs. As a consequence a lack of covergence or convergence to the wrong fixed point may occur. This is especially likely in the case of time-like iteration to steady-state where an arbitary initial condition is imposed.

- The bifurcation of spirals to limit cycles which might account, in part for the phenomenon of near (but lack of) convergence in large systems.

It should always be bourne in mind that although in our illustrations, due to their relatively simple nature and the manner of presentation of results (i.e. full representation of parameter space), the spurious dynamics has been readily detected; this will not always be the case in practical computations especially where higher order systems are involved.

6 Acknowledgements

We would like to thank David Griffiths (University of Dundee) and Andrew Stuart (University of Bath) for the many useful discussions during the course of this work and for suggesting the model equations (12) and (13).

Appendices

A Computations of orbits and bifuractions

The calculations carried out in this work were performed on a Connection Machine CM2 which is a parallel machine with 65,536 processors. The computational domain is considered as a 512×512 array of pixels, the value of the computational variables being taken at the center of each pixel.

The calculation of the bifurcation diagrams and the orbits is essentially the same, the only difference being the computational space ((r, u) or (u, v)) in which we are working. Initially the pixel variables are assigned values according to their position in computational space and constant v or r as

appropriate. The numerical scheme is then applied to these values for an initial number of iterations (typically 1000) to allow the solution trajectories to reach their asymptotic states. At this stage the pixel variables will not have their initial (u, v) values, unless the pixel represents a fixed point or belongs to a periodic orbit. That is, if an initial value lies on a periodic orbit it will visit itself again at some later point in time. (A tolerance of half a pixel width is allowed, the initial number of iterations preventing mistaken identity of slowly varying trajectories.) Such points are marked on the raster display, and a further number of iterations taken, this time checking against initial conditions at each step, to identify all other such points. Due to the finite number of pixels and the form of the tolerance test high order periods will be detected, although they will appear as lower order periods due to the resolution.

The basins of attraction for both the bifurcation diagrams and the phase orbits are calculated in a similar manner by use of a reference point. For the bifurcation diagram case this point is $(r, u_{\min})$ where $u_{\min}$ is the minimum value of u on the orbit for which $v = 0$ and for the phase portraits the reference point is taken as $(u_{\min}, v(u_{\min}))$ where here $u_{\min}$ is the minimum value of u on the orbit. If the pixel values take the value of a reference point during the calculations then the pixel is coloured accordingly. (In practice the reference values are calculated at the same time being replaced whenever a point with smaller u value is found on the orbit.) Note that the reference values must belong to the orbits and so are found using the same techniques as above.

References

[1] Abraham, R.H. & Shaw, C.D. *Dynamics: The Geometry of Behaviour (3 vols)*Aerial Press, Snata Cruz, CA 1982,3,5

[2] Andronov, A.A., Leontovich, E.A., Gordon, I.I. & and Maier A.G. *Theory of Bifurcations of Dynamic Systems on a Plan,* Israel Program for Scientific Translations Ltd., 1971, U.S. Department of Commerce, National Information Service, Springfield, Va. 22151.

[3] Andronov, A.A., Leontovich, E.A., Gordon, I.I. & and Maier A.G. *Qualitative Theory of Second-Order Dynamic Systems,*A. Halsted press book, John Wiley & Sons, New York, 1973.

[4] Chow, S.N. & Hale, J.K. *Methods of Bifurcation Theory,* Springer–Verlag 1982

[5] DERIVE Computer algebraic manipulation package.

[6] Griffiths, D.F., Stuart, A.M. & Yee, H.C. *Numerical Wave Propagation in Hyperbolic Problems with Nonlinear Source Terms,* University of Bath Report, March 1991

[7] Griffith, D.F., Sweby, P.K. & Yee, H.C. *On Spurious Asymptotic Numerical Solutions of Explicit Runge-Kutta Schemes,* to appear IMA J. Numer. Anal.

[8] Guckenheimer, J. & Holmes, P. *Nonlinear Oscillations, Dynamical Systems, and Bifurcations of Vector Fields,* Springer–Verlag 1983

[9] Hairer, E., Iserles, A. & Sanz-Serna, J.M. *Equilibria of Runge-Kutta Methods,* 1989, to appear NUmer. Math.

[10] Humphries, A.R. *Spurious Solutions of Numerical Methods for Initial Value Problems,* Submitted IMA J. Num. Anal. 1991

[11] Iserles, A. *Stability and Dynamics of Numerical Methods for Nonlinear Ordinary Differential Equations,* IMA J. Numer. Anal., **10** 1990

[12] Lafon, A. & Yee, H.C. *Dynamical Approach Study of Spurious Steady-State Numerical Solutions for Nonlinear Differential Equations, Part III, The Effects of Nonlinear Source Terms and Boundary Conditions in Reaction-Convection Equations,* NASA TM 103877, July 1991

[13] Lafon, A. & Yee, H.C. *Dynamical Approach Study of Spurious Steady-State Numerical Solutions for Nonlinear Differential Equations, Part IV, Stability vs. Numerical Treatment of Nonlinear Source Terms,* NASA TM in preparation 1991

[14] Lambert, J.D. *Numerical Methods for Ordinary Differential Systems,* Wiley 1991

[15] MAPLE Computer algebraic manipulation package.

[16] MATHEMATICA Computer algebraic manipulation package.

[17] Sweby, P.K., Yee, H.C & Griffiths, D.F. *On Spurious Steady-State Solutions of Explicit Runge-Kutta Schemes,* University of Reading Numerical Analysis Report 3/90, also NASA TM 102819, April 1990.

[18] Yee, H.C. & Sweby, P.K. *Dynamical Approach Study of Spurious Steady-State Numerical Solutions for Nonlinear Differential Equations, Part II, The Dynamics of Numerics of* 2×2 *ODEs and its Connection to Finite Discretizations of PDEs,* NASA TM in preparation 1991

[19] Yee, H.C., Sweby, P.K. & Griffiths, D.F. *Dynamical Approach Study of Spurious Steady-State Numerical solutions for Nonlinear Differential Equations, Part I, The Dynamics of Time Discretizations and its Implications for Algorithm Development in Computational Fluid Dynamics,* NASA TM 102820, April 1990, to appear J. Comput. Phys., 1991